

---

# EVALUATING THE ROBUSTNESS OF INTERPRETABILITY METHODS THROUGH EXPLANATION INVARIANCE AND EQUIVARIANCE

---

**Jonathan Crabbé**  
DAMTP  
University of Cambridge  
jc2133@cam.ac.uk

**Mihaela van der Schaar**  
University of Cambridge  
Alan Turing Institute  
mv472@cam.ac.uk

## ABSTRACT

Interpretability methods are valuable only if their explanations faithfully describe the explained model. In this work, we consider neural networks whose predictions are invariant under a specific symmetry group. This includes popular architectures, ranging from convolutional to graph neural networks. Any explanation that faithfully explains this type of model needs to be in agreement with this invariance property. We formalize this intuition through the notion of explanation invariance and equivariance by leveraging the formalism from geometric deep learning. Through this rigorous formalism, we derive (1) two metrics to measure the robustness of any interpretability method with respect to the model symmetry group; (2) theoretical robustness guarantees for some popular interpretability methods and (3) a systematic approach to increase the invariance of any interpretability method with respect to a symmetry group. By empirically measuring our metrics for explanations of models associated with various modalities and symmetry groups, we derive a set of 5 guidelines to allow users and developers of interpretability methods to produce robust explanations.

## 1 Introduction

With their increasing success in various tasks, such as computer vision [75], natural language processing [70] and scientific discovery [34], deep neural networks (DNNs) have become widespread. State of the art DNNs typically contain millions to billions parameters and, hence, it is unrealistic for human users to precisely understand how these models issue predictions. This opacity increases the difficulty to anticipate how models will perform when deployed [48]; distil knowledge from the model [21] and gain the trust of stakeholders in high-stakes domains [13, 46]. To address these shortcomings, the field of *interpretable machine learning* has received increasing interest [1, 6]. There exists mainly 2 approaches to increase model interpretability [59]. (1) Restrict the model’s architecture to *interpretable architectures*. For instance, attention models explain their predictions by highlighting features or hidden states they pay attention to [14, 3] and prototype-based models motivate their predictions by highlighting related examples from their training set [12]. (2) Use *post-hoc* interpretability methods in a plug-in fashion after training the model. The advantage of this approach is that it requires no assumption on the model that we need to explain. Post-hoc interpretability includes *feature importance* methods (also known as feature attribution or saliency) that highlight features the model is sensitive to [56, 49]; *example importance* methods that identify influential training examples [43, 25] and *concept-based explanations* that exhibit how classifiers relate classes to human friendly concepts [39, 17]. In this work, we focus on post-hoc interpretability.

With the multiplication of interpretability methods, it has become necessary to evaluate the quality of their explanations [29]. This stems from the fact that interpretability methods need to faithfully describe the model in order to provide actionable insights. Existing approaches to evaluate the quality of interpretability methods fall in 2 categories [21, 80]. (1) Human-centred evaluation investigate how the explanations help humans (experts or not) to anticipate the model’s predictions [45] and whether the model’s explanations are in agreement with some notion of ground-truth [76, 60, 19]. (2) Functionality-grounded evaluation measure the explanation quality based on some desirable properties and do not require humans to be involved. Most of the existing work in this category measure the *robustness* of interpretability

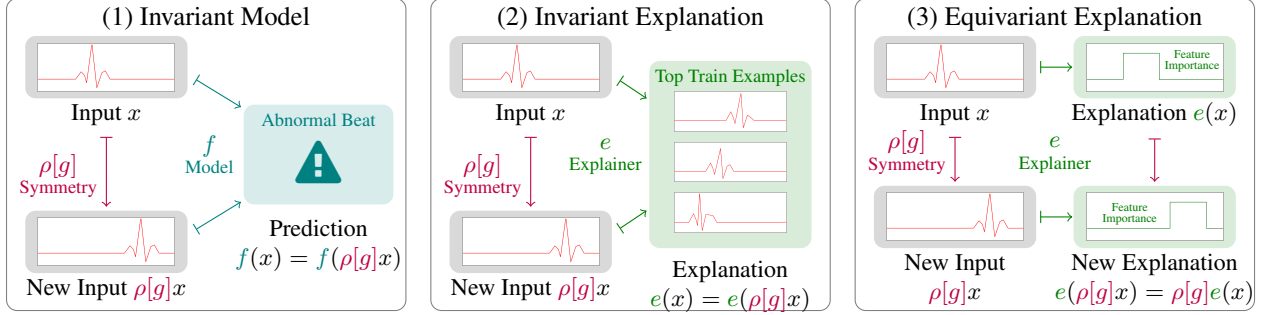


Figure 1: Illustration of model invariance and explanation invariance/equivariance with the simple case of an electrocardiogram (ECG) signal. In this case, the heartbeat described by the ECG remains the same if we apply any translation symmetry with periodic boundary conditions. (1) A model is invariant under the symmetry if the model’s prediction are not affected by the symmetry we apply to the signal. In this case, the model identifies an abnormal heartbeat before and after applying a translation. Any explanation that faithfully describes the model should reflect this symmetry. (2) For some explanations, the right behaviour is to be invariant as well. For instance, the most influential examples for the prediction should be the same for the original and the transformed signal, since the model makes no difference between the two signals. (3) For other type of explanations, the right behaviour is to be equivariant. For instance, the most important part of the signal for the prediction should be the same for the original and the transformed signal, since the model makes no difference between the two signals. Hence, the saliency map undergoes the same translation as the one applied to the signal.

methods with respect to transformations of the model input that should not impact the explanation [53]. Since our work falls in this category, let us now summarize the relevant literature.

**Related Works.** [40] showed that feature importance methods are sensitive to constant shifts in the model’s input. This is unexpected because these constant shifts do not contribute to the model’s prediction. Building on this idea of invariance of the explanations with respect to input shifts, [4, 77, 8] propose a *sensitivity* metric to measure the robustness of feature importance methods based on their stability with respect to small perturbations of the model input. By optimizing small adversarial perturbations, [20, 26, 32] show that imperceptible changes in the input can change the feature importance arbitrarily by approximately keeping the model prediction constant. This shows that many interpretability methods, as neural networks, are sensitive to adversarial perturbations. Subsequent works have addressed this pathologic behaviour by fixing the model training dynamic. In particular, they showed that penalizing large eigenvalues of the training loss Hessian with respect to the inputs make the interpretations of this model more robust with respect to adversarial attacks [72, 2]. To the best of our knowledge, the only work that discusses the behaviour of explanations under more general transformations of the input data is [71]. However, the work’s focus is more on model regularization rather than on the evaluation of post-hoc interpretability robustness.

**Motivations.** In reviewing the above literature, we notice 3 gaps. (1) The existing studies mostly focus on evaluating feature importance methods. In spite of the predominance of feature importance in the literature [5], we note that other types of interpretability methods exist and deserve to be analyzed. (2) The existing studies mostly focus on images. While computer vision is undoubtedly an interesting application of DNNs, it would be interesting to extend the analysis to other modalities, such as times series and graph data [74]. (3) The existing studies mostly focus on simple transformation of the model input, such as small shifts. This is motivated by the fact that the predictions of DNNs are mostly invariant under these transformations. Again, this is another direction that could be explored more thoroughly as numerous DNNs are also invariant to more complex transformation of their input data. For instance, graph neural networks are invariant to permutations of the node ordering in their input graph [38]. Our work proposes to further investigate the robustness of interpretability methods by following these 3 directions.

**Contributions.** We propose a new framework to evaluate the robustness of interpretability methods. We consider a setting where the model we wish to interpret is invariant with respect to a group  $\mathcal{G}$  of symmetry acting on the model input. Any explanation that faithfully describes this model should have explanations that are conserved by this group of symmetry  $\mathcal{G}$ . We illustrate this reasoning in Figure 1 with the simple group  $\mathcal{G}$  of time translations acting on the input signal. With this new framework, we bring several contributions. (1) **Rigorous Interpretability Robustness.** We define interpretability robustness with respect to a group  $\mathcal{G}$  of symmetry through explanation invariance and equivariance. In agreement with our motivations, we demonstrate in Section 2.2 that our general definitions cover different type of interpretability methods, modalities and transformations of the input data. (2) **Evaluation of Interpretability**

**Methods.** Not all interpretability methods are equal with respect to our notion of robustness. In Section 2.3, we show that some popular interpretability methods are naturally endowed with theoretical robustness guarantees. Further, we introduce 2 metrics, the invariance and equivariance scores, to empirically evaluate this robustness. In Section 3.1, we use these metrics to evaluate the robustness of 3 types of interpretability methods with 3 different model types corresponding to 3 different modalities and symmetry groups. Our empirical results support our theoretical analysis. **(3) Insights to Improve Robustness.** By combining our theoretical and empirical analysis, we derive a set of 5 actionable guidelines to ensure that interpretability methods are used in a way that guarantees robustness with respect to the symmetry group  $\mathcal{G}$ . In particular, we show in Sections 2.3 and 3.2 that we can improve the invariance score of any interpretability method by aggregating explanations over various symmetries. We summarize the guidelines with a flowchart in Figure 5, that helps users to improve the robustness of their interpretability methods.

## 2 Interpretability Robustness

In this section, we formalize the notion of interpretability robustness through explanation invariance and equivariance. We start with a reminder of some useful definitions from geometric deep learning. We then define two metrics to measure the invariance and equivariance of interpretability methods. We leverage this formalism to derive some theoretical robustness guarantees for popular interpretability methods. Finally, we describe a rigorous approach to improve the invariance of any interpretability method.

### 2.1 Useful Notions of Geometric Deep Learning

Some basic concepts of group theory are required for our definition of interpretability robustness. To that aim, we leverage the formalism of *Geometric Deep Learning*. Please refer to [10] for more details. To rigorously define explanation equivariance and invariance, we need some form of structure in the data we are manipulating. This precludes tabular data but includes graph, time series and image data. In this setting, the data is defined on a finite domain set  $\Omega$  (e.g. a grid  $\Omega = \mathbb{Z}_n \times \mathbb{Z}_n$  for  $n \times n$  images). On this domain, the data is represented by signals  $x \in \mathcal{X}(\Omega, \mathcal{C})$ , mapping each point  $u \in \Omega$  of the domain to a channel vector  $x(u) \in \mathcal{C} = \mathbb{R}^{d_C}$ . We note that  $d_C \in \mathbb{N}^+$ , corresponds to the number of channels of the signal (e.g.  $d_C = 3$  for RGB images). The set of signals has naturally the structure of a vector space since  $x_1, x_2 \in \mathcal{X}(\Omega, \mathcal{C}) \Rightarrow \lambda_1 \cdot x_1 + \lambda_2 \cdot x_2 \in \mathcal{X}(\Omega, \mathcal{C})$  for all  $\lambda_1, \lambda_2 \in \mathbb{R}$ .

**Symmetries.** Informally, symmetries are transformations of the data that leave the information content unchanged (e.g. moving an image one pixel to the right). More formally, symmetries correspond to a set  $\mathcal{G}$  endowed with a composition operation  $\circ : \mathcal{G}^2 \rightarrow \mathcal{G}$ . Clearly, this set  $\mathcal{G}$  includes an identity transformation  $id$  that leaves the data untouched. Similarly, if a transformation  $g \in \mathcal{G}$  preserves the information, then it could be undone by an inverse transformation  $g^{-1} \in \mathcal{G}$  such that  $g^{-1} \circ g = id$ . Those properties<sup>1</sup> give  $\mathcal{G}, \circ$  the structure of a *group*. In this paper, we assume that the symmetry group has a *finite* number of elements.

**Group Representation.** We have yet to formalize how the above symmetries transform the data. To that aim, we need to link the symmetry group  $\mathcal{G}$  with the signal vector space  $\mathcal{X}(\Omega, \mathcal{C})$ . This connection is achieved by choosing a *group representation*  $\rho : \mathcal{G} \rightarrow \text{Aut}[\mathcal{X}(\Omega, \mathcal{C})]$  that maps each symmetry  $g \in \mathcal{G}$  to an *automorphism*  $\rho[g] \in \text{Aut}[\mathcal{X}(\Omega, \mathcal{C})]$ . Formally, the automorphisms  $\text{Aut}[\mathcal{X}(\Omega, \mathcal{C})]$  are defined as bijective linear transformations mapping  $\mathcal{X}(\Omega, \mathcal{C})$  onto itself. In practice, each automorphism  $\rho[g]$  is represented by an invertible matrix acting on the vector space  $\mathcal{X}(\Omega, \mathcal{C})$ . For instance, an image translation  $g$  can be represented by a permutation matrix  $\rho[g]$ . To qualify as a group representation, the map  $\rho$  needs to be compatible with the group composition:  $\rho[g_2 \circ g_1] = \rho[g_2]\rho[g_1]$ . This property guarantees that the composition of two symmetries can be implemented as the multiplication between two matrices.

**Invariance.** We first consider the case of a deep neural network  $f : \mathcal{X}(\Omega, \mathcal{C}) \rightarrow \mathcal{Y}$ , where the output  $f(x) \in \mathcal{Y}$  is a vector with no underlying structure (e.g. class probabilities for a classifier). In this case, we expect the model’s prediction to be unchanged when applying a symmetry  $g \in \mathcal{G}$  to the input signal  $x \in \mathcal{X}(\Omega, \mathcal{C})$ . For instance, the probability of observing a cat on an image should not change if we move the cat by one pixel to the right. This intuition is formalized by defining the  $\mathcal{G}$ -*invariance* property for the model  $f$ :  $f(\rho[g]x) = f(x)$  for all  $g \in \mathcal{G}, x \in \mathcal{X}(\Omega, \mathcal{C})$ .

**Equivariance.** We now turn to the case of deep neural networks  $f : \mathcal{X}(\Omega, \mathcal{C}) \rightarrow \mathcal{Y}(\Omega', \mathcal{C}')$ , where the output  $f(x) \in \mathcal{Y}(\Omega', \mathcal{C}')$  is also a signal (e.g. segmentation masks for an object detector). We note that the domain  $\Omega'$  and the channel space  $\mathcal{C}'$  are not necessarily the same as  $\Omega$  and  $\mathcal{C}$ . When applying a transformation  $g \in \mathcal{G}$  to the input signal  $x \in \mathcal{X}(\Omega, \mathcal{C})$ , it is legitimate to expect the output signal  $f(x)$  to follow a similar transformation. For instance, the segmentation of a cat on an image should move by one pixel to the right if we move the cat by one pixel to the right. This intuition is formalized by defining the  $\mathcal{G}$ -*equivariance* property for the model  $f$ :  $f(\rho[g]x) = \rho'[g]f(x)$ . Again,

<sup>1</sup>Note that groups also satisfy associativity:  $g_1 \circ (g_2 \circ g_3) = (g_1 \circ g_2) \circ g_3$  for all  $g_1, g_2, g_3 \in \mathcal{G}$ .

the representation  $\rho' : \mathcal{G} \rightarrow \text{Aut}[\mathcal{Y}(\Omega', \mathcal{C}')] ]$  is not necessarily the same as the representation  $\rho$  since the signal spaces  $\mathcal{X}(\Omega, \mathcal{C})$  and  $\mathcal{Y}(\Omega', \mathcal{C}')$  might have different dimensions.

## 2.2 Explanation Invariance and Equivariance

We will now restrict to models that are  $\mathcal{G}$ -invariant. It is legitimate to expect similar invariance properties for the explanations associated to this model. We shall now formalize this idea for generic explanations. We assume that explanations are functions of the form  $e : \mathcal{X}(\Omega, \mathcal{C}) \rightarrow \mathcal{E}$ , where  $\mathcal{E} \subseteq \mathbb{R}^{d_E}$  is an explanation space with  $d_E \in \mathbb{N}^+$  dimensions<sup>2</sup>.

**Invariance and Equivariance.** The invariance and equivariance of the explanation  $e$  with respect to symmetries  $\mathcal{G}$  are defined as in the previous section. In this way, we say that the explanation  $e$  is  $\mathcal{G}$ -invariant if  $e(\rho[g]x) = e(x)$  and  $\mathcal{G}$ -equivariant if  $e(\rho[g]x) = \rho'[g]e(x)$  for all  $g \in \mathcal{G}, x \in \mathcal{X}(\Omega, \mathcal{C})$ . There is no reason to expect these equalities to hold exactly a priori. This motivates the introduction of two metrics that measure the violation of explanation invariance and equivariance by an interpretability method.

**Definition 2.1** (Robustness Metrics). Let  $f : \mathcal{X}(\Omega, \mathcal{C}) \rightarrow \mathcal{Y}$  be a neural network that is invariant with respect to the symmetry group  $\mathcal{G}$  and  $e : \mathcal{X}(\Omega, \mathcal{C}) \rightarrow \mathcal{E}$  be an explanation for  $f$ . We assume that  $\mathcal{G}$  acts on  $\mathcal{X}(\Omega, \mathcal{C})$  via the representation  $\rho : \mathcal{G} \rightarrow \text{Aut}[\mathcal{X}(\Omega, \mathcal{C})]$ . We measure the *invariance* of  $e$  with respect to  $\mathcal{G}$  for some  $x \in \mathcal{X}(\Omega, \mathcal{C})$  with the metric

$$\text{Inv}_{\mathcal{G}}(e, x) \equiv \frac{1}{|\mathcal{G}|} \sum_{g \in \mathcal{G}} s_{\mathcal{E}} [e(\rho[g]x), e(x)], \quad (1)$$

where  $s_{\mathcal{E}} : \mathcal{E}^2 \rightarrow \mathbb{R}$  is a similarity score on the explanation space  $\mathcal{E}$ . We use the cos-similarity  $s_{\mathcal{E}}(a, b) = a^{\top}b / \|a\|_2 \cdot \|b\|_2$  for real-valued explanations  $a, b \in \mathbb{R}^{d_E}$  and the accuracy score  $s_{\mathcal{E}}(a, b) = d_E^{-1} \sum_{i=1}^{d_E} \mathbb{1}(a_i = b_i)$  for categorical explanations  $a, b \in \mathbb{Z}_K^{d_E}$ , where  $\mathbb{1}$  is the indicator function and  $K \in \mathbb{N}^+$  is the number of categories. If we assume that  $\mathcal{G}$  acts on  $\mathcal{E}$  via the representation  $\rho' : \mathcal{G} \rightarrow \text{Aut}[\mathcal{E}]$ , we measure the *equivariance* of  $e$  with respect to  $\mathcal{G}$  for some  $x \in \mathcal{X}(\Omega, \mathcal{C})$  with the metric

$$\text{Equiv}_{\mathcal{G}}(e, x) \equiv \frac{1}{|\mathcal{G}|} \sum_{g \in \mathcal{G}} s_{\mathcal{E}} [e(\rho[g]x), \rho'[g]e(x)]. \quad (2)$$

A score  $\text{Inv}_{\mathcal{G}}(e, x) = 1$  or  $\text{Equiv}_{\mathcal{G}}(e, x) = 1$  indicates that the explanation method  $e$  is  $\mathcal{G}$ -invariant or equivariant for the example  $x \in \mathcal{X}(\Omega, \mathcal{C})$ .

*Remark 2.2.* The metrics  $\text{Inv}_{\mathcal{G}}$  and  $\text{Equiv}_{\mathcal{G}}$  might be prohibitively expensive to evaluate whenever the size  $|\mathcal{G}|$  of the symmetry group  $\mathcal{G}$  is too big. Note that this is typically the case in our experiments as we consider large permutation groups of order  $|\mathcal{G}| \gg 10^{32}$ . In this case, we use Monte Carlo estimators for both metrics by uniformly sampling  $G \sim U(\mathcal{G})$  and averaging over a number of sample  $N_{\text{samp}} \ll |\mathcal{G}|$ . We study the convergence of those Monte Carlo estimators in Appendix C.

The above approach to measure the robustness of interpretability method applies to a wide variety of settings. To clarify this, we explain how to adapt the above formalism to 3 popular types of interpretability methods: *feature importance*, *example importance* and *concept-based explanations*.

**Feature Importance.** Feature importance explanations associate a saliency map  $e(x) \in \mathcal{X}(\Omega, \mathcal{C})$  to each example  $x \in \mathcal{X}(\Omega, \mathcal{C})$  for the model's prediction  $f(x)$ . In this case, we note that the explanation space corresponds to the model's input space  $\mathcal{E} = \mathcal{X}(\Omega, \mathcal{C})$ , since the method assigns an importance score to each individual feature. If we apply a symmetry to the input, we expect the same symmetry to be applied to the saliency map, as illustrated by the example from Figure 1. Hence, the most relevant metric to record here is the explanation equivariance  $\text{Equiv}_{\mathcal{G}}$ . Since the input space and the explanation space are identical  $\mathcal{E} = \mathcal{X}(\Omega, \mathcal{C})$ , we work with identical representations  $\rho' = \rho$ . We note that this metric generalizes the self-consistency score introduced by [71] beyond affine transformations.

**Example Importance.** Example importance explanations associate an importance vector  $e(x) \in \mathbb{R}^{N_{\text{train}}}$  to each example  $x \in \mathcal{X}(\Omega, \mathcal{C})$  for the model's prediction  $f(x)$ . Note that  $N_{\text{train}} \in \mathbb{N}^+$  is typically the model's training set size, so that each component of  $e(x)$  corresponds to the importance of a training example. If we apply a symmetry to the input, we expect the relevance of training examples to be conserved, as illustrated by the example from Figure 1. Hence, the most relevant metric to record here is the invariance  $\text{Inv}_{\mathcal{G}}$ .

**Concept-Based Explanations.** Concept-based explanations associate a binary concept presence vector  $e(x) \in \{0, 1\}^C$  to each example  $x \in \mathcal{X}(\Omega, \mathcal{C})$  for the model's prediction  $f(x)$ . Note that  $C \in \mathbb{N}^+$  is the number of concepts one

<sup>2</sup>Note that the explanation  $e$  also depends on the model  $f$ . Since the model is fixed, we make this dependency implicit.

considers, so that each component of  $e(x)$  corresponds to the presence/absence of a concept. If we apply a symmetry to the input, there is no reason for a concept to appear/vanish, since the information content of the input is untouched by the symmetry. Hence, the most relevant metric to record here is again the invariance  $\text{Inv}_{\mathcal{G}}$ .

### 2.3 Theoretical Analysis

Table 1: Theoretical robustness guarantees that we derive for explanations of invariant models. We split the interpretability methods according to their type (feature importance, example importance or concept-based) and according to model information they rely on (model gradients, perturbations, loss or representations). We consider 3 levels of guarantees: ✓ indicates unconditional guarantee, ~ conditional guarantee and ✗ no guarantee.

TYPE	COMPUTATION	EXAMPLE	INVARIANT	EQUIVARIANT	DETAILS
FEATURE IMPORTANCE	GRAD. $\nabla_x f(x)$	[66]	✗	~	PROP. B.6
	PERT. $f(x + \delta x)$	[24]	✗	~	PROP. B.8
EXAMPLE IMPORTANCE	LOSS $\mathcal{L}[f(x), y]$	[43]	✓	✗	PROP. B.9
	REP. $h(x)$	[18]	~	✗	PROP. B.12
CONCEPT-BASED	REP. $h(x)$	[39]	~	✗	PROP. B.14

Let us now provide a theoretical analysis of robustness in a setting where the model  $f$  is  $\mathcal{G}$ -invariant. We first show that many popular interpretability methods naturally offer some robustness guarantee if we make some assumptions. For methods that are not invariant when they should, we propose an approach to enforce  $\mathcal{G}$ -invariance.

**Robustness Guarantees.** In Table 1, we summarize the theoretical robustness guarantees that we derive for popular interpretability methods. All of these guarantees are formally stated and proven in Appendix B. We emphasize that these guarantees make assumptions that typically restrict the type of representation  $\rho$  to manipulate, the kind of baseline signal  $\bar{x} \in \mathcal{X}(\Omega, \mathcal{C})$  used by attribution methods and the layer of the model  $f$  that is used to derive the explanations.

**Enforcing Invariance.** If the explanation  $e$  is not  $\mathcal{G}$ -invariant when it should, we can construct an auxiliary explanation  $e_{\text{inv}}$  built upon  $e$  that is  $\mathcal{G}$ -invariant. This permits to improve the robustness of any interpretability method that has no invariance guarantee. The idea is simply to aggregate the explanation over several symmetries.

**Proposition 2.3.** [Enforce Invariance] Consider a neural network  $f : \mathcal{X}(\Omega, \mathcal{C}) \rightarrow \mathcal{Y}$  that is invariant with respect to the symmetry group  $\mathcal{G}$  and  $e : \mathcal{X}(\Omega, \mathcal{C}) \rightarrow \mathcal{E}$  be an explanation for  $f$ . We assume that  $\mathcal{G}$  acts on  $\mathcal{X}(\Omega, \mathcal{C})$  via the representation  $\rho : \mathcal{G} \rightarrow \text{Aut}[\mathcal{X}(\Omega, \mathcal{C})]$ . We define the auxiliary explanation  $e_{\text{inv}} : \mathcal{X}(\Omega, \mathcal{C}) \rightarrow \mathcal{E}$  as

$$e_{\text{inv}}(x) \equiv \frac{1}{|\mathcal{G}|} \sum_{g \in \mathcal{G}} e(\rho[g]x)$$

for all  $x \in \mathcal{X}(\Omega, \mathcal{C})$ . The auxiliary explanation  $e_{\text{inv}}$  is invariant under the symmetry group  $\mathcal{G}$ .

*Proof.* Please refer to Appendix B. □

*Remark 2.4.* Once again, a Monte Carlo estimation for  $e_{\text{inv}}$  might be required for groups  $\mathcal{G}$  with many elements. This produces explanations that are approximatively invariant.

## 3 Experiments

In this section, we use our interpretability robustness metrics to draw some insights from real-world models and datasets. We first evaluate the  $\mathcal{G}$ -invariance and equivariance of popular interpretability methods used on top of a  $\mathcal{G}$ -invariant model. With this analysis, we identify interpretability methods that are not robust. We then show that the robustness of these interpretability methods can largely be improved by using their auxiliary version defined in Proposition 2.3. Finally, we study how the  $\mathcal{G}$ -invariance and equivariance of interpretability methods varies when we decrease the invariance of the underlying model. From these experiments, we derive 5 guidelines to ensure that interpretability methods are robust with respect to symmetries from  $\mathcal{G}$ . We summarize these guidelines with a flowchart in Figure 5. More details on the experiments are available in Appendix D. We also include a comparison between our robustness metrics and the sensitivity metric in Appendix E. The code to replicate all the results reported in the paper is available in <https://github.com/JonathanCrabbe/RobustXAI>.

**Datasets.** We use 3 different datasets to illustrate various modalities and symmetry groups. **Electrocardiograms.** The MIT-BIH Electrocardiogram (ECG) dataset [27, 50] consists of univariate time series  $x \in \mathcal{X}(\mathbb{Z}_T, \mathbb{R})$  with  $T = 187$  time

steps, each representing a heartbeat cycle. Each time series comes with a binary label indicating whether the heartbeat is normal or not. We train a 1-dimensional convolutional neural network (CNN) to predict this label. This CNN is made invariant under the action of the cyclic translation group  $\mathcal{G} = \mathbb{Z}/T\mathbb{Z}$  on the time series by using only circular padding and global pooling. **Mutagenicity.** The Mutagenicity dataset [37, 57, 52] consists of graphs  $x \in \mathcal{X}([V_x, E_x], \mathbb{Z}_{N_{\text{sp}}})$  representing organic molecules. In a graph, each node  $u \in V_x$  is assigned an atom indexed by  $x(u) \in \mathbb{Z}_{N_{\text{sp}}}$ , where  $N_{\text{sp}} = 14$  is the number of atom species. We ignore the attributes for the edges  $E_x \subseteq V_x^2$ . Each graph comes with a binary label indicating whether the molecule is a mutagen or not. We train a graph neural network (GNN) to predict this label. This GNN is made invariant under the action of the permutation group  $\mathcal{G} = S_{V_x}$  on the node ordering by using global pooling. **ModelNet40.** The ModelNet40 [73] dataset consists of CAD representations of 3D objects. We use the same process as Zaheer et al. [78], Lee et al. [47] to convert each CAD representation into a cloud  $x \in \mathcal{X}(\mathbb{Z}_{N_{\text{pt}}}, \mathbb{R}^3)$  of  $N_{\text{pt}} = 1,000$  points embedded in  $\mathbb{R}^3$ . Each cloud of point comes with a label  $y \in \mathbb{Z}_{40}$  indicating the class of object represented by the cloud of points among the 40 different classes of objects present in the dataset. We train a Deep Set [78] model to predict this label. Thanks to its architecture, this model is naturally invariant under the action of the permutation group  $\mathcal{G} = S_{N_{\text{pt}}}$  on the points in the cloud. Each model is trained on a training set  $\mathcal{D}_{\text{train}}$ . For details of the architectures and the training process, please refer to Appendix D.

**Explanations.** In each setting, we explain the model predictions with 3 popular types of interpretability methods. **Feature Importance.** We study gradient-based methods with Integrated Gradients [66] and Gradient Shap [49] as well as perturbation-based methods with Feature Ablation, Permutation [24] and Occlusion [79]. Whenever a baseline is required, we consider the trivial signal  $\bar{x} = 0$  as a baseline. We note that this signal is trivially  $\mathcal{G}$ -invariant as  $\rho[g]\bar{x} = 0$  for all  $g \in \mathcal{G}$ . **Example Importance.** We study loss-based methods with Influence Functions [43] and TraIn [25] as well as representation-based methods with SimplEx [18] and Representation Similarity. Since loss-based methods are expensive to compute, we differentiate the loss only with respect to the last layer of each model and for a subset of  $N_{\text{train}} = 100$  training examples from  $\mathcal{D}_{\text{train}}$ . For representation-based methods, we use the output of both invariant and equivariant layers of the model as representation spaces. We denote e.g. SimplEx-Inv to indicate that SimplEx was used by using the output of a  $\mathcal{G}$ -invariant layer of the model as a representation space. Similarly, SimplEx-Equiv corresponds to SimplEx used with the output of a  $\mathcal{G}$ -equivariant layer as a representation space. **Concept-Based Explanations.** To the best of our knowledge, the only 2 post-hoc concept explanation methods in the literature are CAV [39] and CAR [17]. We use these methods to probe the representations of our models through a set of  $C = 4$  concepts specific to each dataset. Again, we use both invariant and equivariant layers of the model for each method. Please refer to Appendix D for further details on the interpretability methods.

### 3.1 Evaluating Interpretability Methods

**Motivation.** The purpose of this experiment is to measure the robustness of various interpretability methods. Since we manipulate models that are invariant with respect to a group  $\mathcal{G}$ ,  $\circ$  of symmetry, we expect feature importance methods to be  $\mathcal{G}$ -equivariant ( $\text{Equiv}_{\mathcal{G}}[e, x] = 1$  for all  $x \in \mathcal{X}(\Omega, \mathcal{C})$ ). Similarly, we expect example and concept-based methods to be  $\mathcal{G}$ -invariant ( $\text{Inv}_{\mathcal{G}}[e, x] = 1$  for all  $x \in \mathcal{X}(\Omega, \mathcal{C})$ ). We shall now verify this empirically.

**Methodology.** To measure the robustness of interpretability methods empirically, we use a set  $\mathcal{D}_{\text{test}}$  of  $N_{\text{test}}$  examples ( $N_{\text{test}} = 433$  for Mutagenicity and  $N_{\text{test}} = 1,000$  in the other cases). For each interpretability method  $e$ , we evaluate the appropriate robustness metric for each test example  $x \in \mathcal{D}_{\text{test}}$ . For the ECG dataset, those metrics are evaluated exactly since  $\mathcal{G}$  has a tractable order  $|\mathcal{G}| = T = 187$ . In the other cases, the large order  $|\mathcal{G}|$  makes the exact evaluation of the metric unrealistic. We therefore use a Monte Carlo approximation with  $N_{\text{samp}} = 50$ . As demonstrated in Appendix C, the Monte Carlo estimators have already converged with this sample size. We note that some interpretability methods cannot be used in some settings. Whenever this is the case, we simply omit the interpretability method. Please refer to Appendix D for more details.

**Analysis.** We report the robustness score for each metric and each dataset on the test set  $\mathcal{D}_{\text{test}}$  in Figure 2. We immediately notice that not all the interpretability methods are robust. When looking at feature importance, we observe that equivariance is not guaranteed by methods that rely on baseline that are not invariant. For instance, Gradient Shap adds Gaussian noise to the baseline  $\bar{x}$ , which breaks the  $\mathcal{G}$ -invariance of the baseline. Similarly, Feature Permutation replaces each feature by randomly resampling the feature within the batch. This is equivalent to using a random baseline, which has no reason to be  $\mathcal{G}$ -invariant. We conclude that the invariance of the baseline  $\bar{x}$  is crucial to guarantee the robustness of feature importance methods. When it comes to example importance, we note that loss-based methods are consistently invariant, which is in agreement with Proposition B.9. Representation-based methods, on the other hand, are invariant only if used with invariant layers of the model. We note a similar behaviour for concept importance explanations. This shows that the choice of what we call the *representation space* matters for these methods. We derive a set of guidelines from these observations.



**Guideline 1.** Feature importance methods should be used with group invariant baseline signal ( $\rho[g]\bar{x} = \bar{x}$  for all  $g \in \mathcal{G}$ ) to guarantee explanation equivariance. Only methods that conserve the invariance of the baseline can guarantee equivariance.

**Guideline 2.** Loss-based example importance methods guarantee explanation invariance, unlike representation-based methods. When using the latter, only invariant layers guarantee explanation invariance.

**Guideline 3.** To guarantee invariance of concept-based explanations, concept classifiers should be used on invariant layers of the model.

### 3.2 Improving Robustness

**Motivation.** In the previous experiment, we noticed that all the interpretability methods are not  $\mathcal{G}$ -invariant when they should. Consider, for instance, concept-based methods used on equivariant layers. The lack of invariance for these methods implies that they rely on concept classifiers that are not  $\mathcal{G}$ -invariant. This behaviour is undesirable for two reasons: (1) since any symmetry  $g \in \mathcal{G}$  preserve the information of a signal  $x \in \mathcal{X}(\Omega, \mathcal{C})$ , the signal  $\rho[g]x$  should contain the same concepts as  $x$  and (2) the layer that we use implicitly encodes these symmetries through equivariance of the output representations. Hence, concept classifiers that are not  $\mathcal{G}$ -invariant fail to generalize by ignoring the symmetries encoded in the structure of the model’s representation space. Fortunately, Proposition 2.3 gives us a prescription to obtain explanations (here concept classifiers) that are more robust with respect to the model’s symmetries. We shall now illustrate how this prescription improves the robustness of concept-based methods.

**Methodology.** In this experiment, we restrict our analysis to the ECG dataset. For each test signal, we sample  $N_{\text{inv}}$  symmetries  $G_1, \dots, G_{N_{\text{inv}}} \in \mathcal{G}$  without replacement. As prescribed by Proposition 2.3, we then compute the auxiliary explanation  $e_{\text{inv}}(x) = N_{\text{inv}}^{-1} \sum_{i=1}^{N_{\text{inv}}} e(\rho[G_i]x)$  for each concept importance method.

**Analysis.** We report the average invariance score  $\mathbb{E}_{X \sim U(\mathcal{D}_{\text{test}})} \text{Inv}_{\mathcal{G}}(e_{\text{inv}}, X)$  for several values of  $N_{\text{inv}}$  in Figure 3. As we can see, the invariance of the explanation grows monotonically with the number of samples  $N_{\text{inv}}$  to achieve a perfect invariance for  $N_{\text{inv}} = |\mathcal{G}|$ . Interestingly, the explanation invariance increases more quickly for CAR. This suggests that enforcing explanation invariance is less expensive for certain interpretability methods and motivates the bellow guideline.

**Guideline 4.** Any interpretability method can be made invariant through Proposition 2.3. In doing so, one should increase the number of samples  $N_{\text{inv}}$  until the desired invariance is achieved. In this way, the method is made robust without increasing the number of calls more than necessary. Note that it only makes sense to enforce invariance of the interpretability method if the explained model is itself invariant.

### 3.3 Relaxing Invariance

**Motivation.** In practice, models are not always perfectly invariant. For instance, CNNs often flatten the output of convolutional layers, which violates translation invariance [64, 36]. Although the resulting models are not perfectly invariant, experiments suggest that CNNs can efficiently learn translation invariance at training time [9]. This motivates to study the invariance/equivariance of interpretability methods used with models that are not perfectly invariant. If the interpretability methods are faithful to the model, we expect their invariance/equivariance to be coupled to the model invariance. We shall now investigate this empirically.

**Methodology.** Again, we restrict our analysis to the ECG dataset. We now manipulate three different models: (1) All-CNN: the perfectly invariant CNN we have manipulated so far. (2) Augmented-CNN: A CNN where the global pooling is replaced by a flatten operation, hence sacrificing invariance. In order for the CNN to learn invariance, we augment

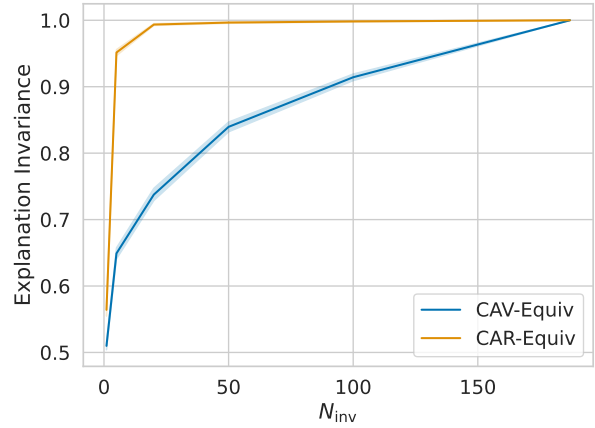


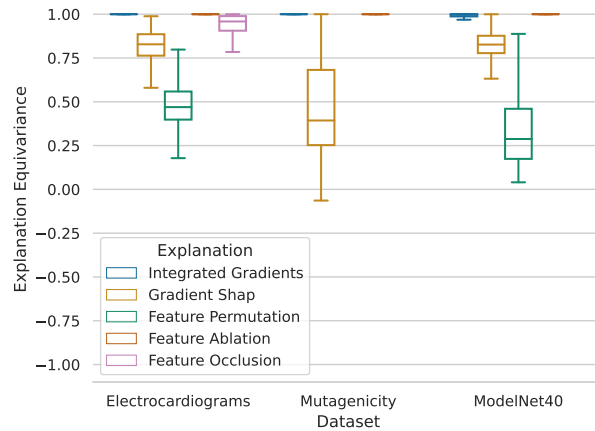
Figure 3: Explanation invariance can be increased according to Proposition 2.3. This plot shows the score averaged on a test set  $\mathcal{D}_{\text{test}}$  together with a 95% confidence interval.

the training set  $\mathcal{D}_{\text{train}}$  by applying random translations at training time. (3) Standard-CNN: Another CNN, with the same architecture as the Augmented-CNN and trained without augmentation. We measure the invariance/equivariance of the interpretability methods for each model. For representation-based methods, we use the output of the first dense layer of the CNN (Lin1). This corresponds to the invariant layer used in Section 3.1.

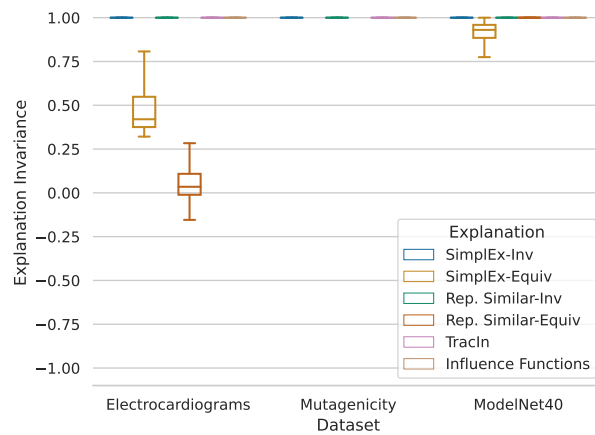
**Analysis.** We report the relationship between model invariance and explanation invariance/equivariance in Figure 4. Unsurprisingly, the most invariant model is the All-CNN, closely followed by the Augmented-CNN and with a Standard-CNN that is noticeably less invariant. We note that in most cases, the invariance/equivariance of the interpretability method substantially increases with the model’s invariance. This is reassuring as it suggests that interpretability methods indeed capture the invariance property from the model. Surprisingly, we note that the drop in invariance is much less important for TraceIn. This method remains largely  $\mathcal{G}$ -invariant regardless of the model’s invariance. This should raise our scepticism as this suggests that, in this case, the explanation invariance results from the interpretability method rather than from the model itself. This motivates our last guideline, which safeguards against erroneous interpretations of our robustness metrics.

**Guideline 5.** When evaluating the robustness of an interpretability method  $e$  with respect to a group of symmetry  $\mathcal{G}$ , one should measure the robustness scores  $\text{Inv}_{\mathcal{G}}(e, \cdot)$  and  $\text{Equiv}_{\mathcal{G}}(e, \cdot)$  both for a  $\mathcal{G}$ -invariant model and for a model that is not  $\mathcal{G}$ -invariant. One can claim that the explanation faithfully captures the model invariance only if its robustness score is substantially higher for the  $\mathcal{G}$ -invariant model.

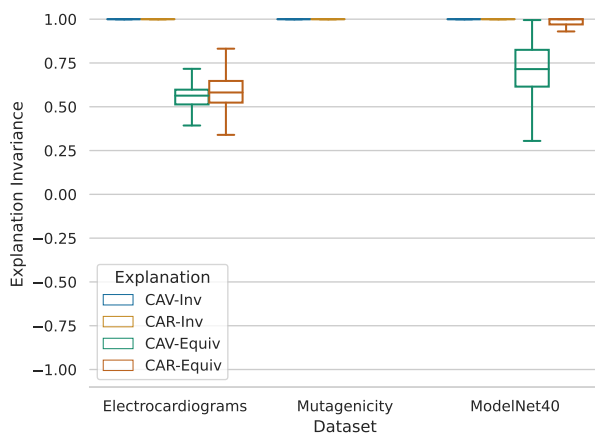




(a) Feature Importance

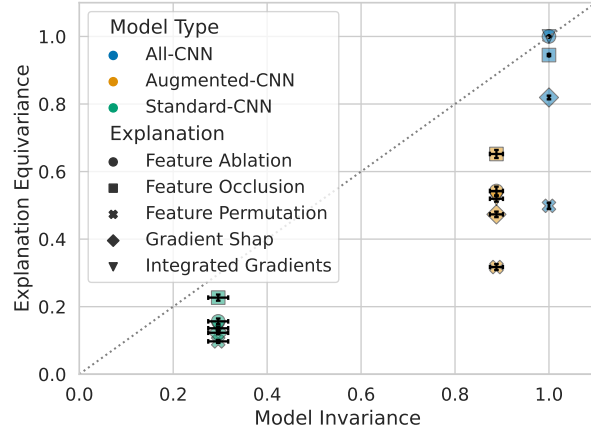


(b) Example Importance

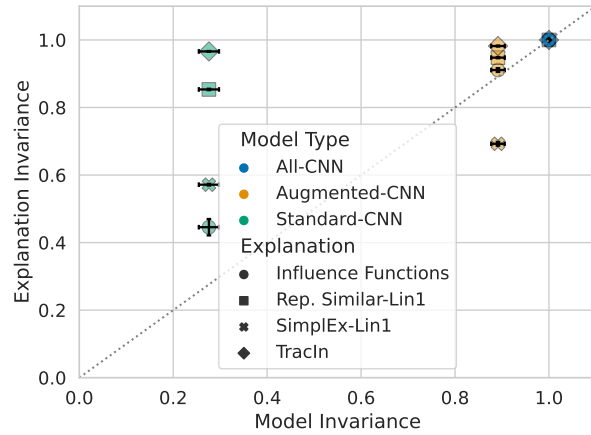


(c) Concept Importance

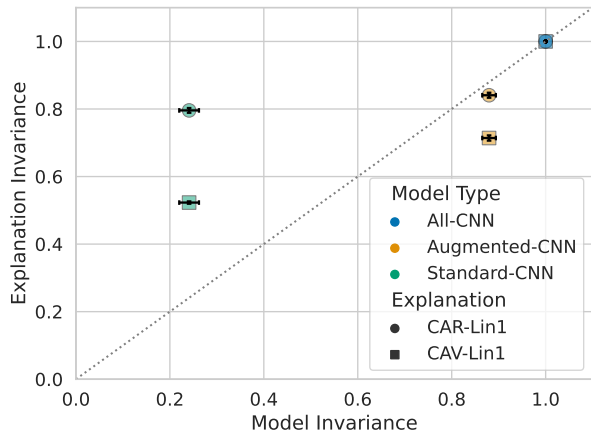
Figure 2: Explanation robustness of interpretability methods for invariant models. The interpretability methods are grouped by type. Each box-plot is produced by evaluating the robustness metrics  $\text{Inv}_{\mathcal{G}}$  or  $\text{Equiv}_{\mathcal{G}}$  across several test samples  $x \in \mathcal{D}_{\text{test}}$ . Any value below 1 for the metrics is unexpected, as the model is  $\mathcal{G}$ -invariant.



(a) Feature Importance



(b) Example Importance



(c) Concept Importance

Figure 4: Effect of relaxing the model invariance on interpretability methods invariance/equivariance. The interpretability methods are grouped by type. The error bars represent a 95% confidence interval around the mean on the test set  $\mathcal{D}_{\text{test}}$  for Inv and Equiv.

## References

- [1] Adadi, A. and Berrada, M. Peeking inside the black-box: A survey on explainable artificial intelligence (xai). *IEEE Access*, 6:52138–52160, 2018. doi:10.1109/ACCESS.2018.2870052.
- [2] Ajalloeian, A., Moosavi-Dezfooli, S.-M., Vlachos, M., and Frossard, P. On smoothed explanations: Quality and robustness. In *Proceedings of the 31st ACM International Conference on Information & Knowledge Management*, pp. 15–25, 2022.
- [3] Alaa, A. M. and van der Schaar, M. Attentive state-space modeling of disease progression. In Wallach, H., Larochelle, H., Beygelzimer, A., d'Alché-Buc, F., Fox, E., and Garnett, R. (eds.), *Advances in Neural Information Processing Systems*, volume 32. Curran Associates, Inc., 2019.
- [4] Alvarez-Melis, D. and Jaakkola, T. S. On the robustness of interpretability methods. *arXiv preprint arXiv:1806.08049*, 2018.
- [5] Arya, V., Bellamy, R. K., Chen, P.-Y., Dhurandhar, A., Hind, M., Hoffman, S. C., Houde, S., Liao, Q. V., Luss, R., Mojsilović, A., et al. One explanation does not fit all: A toolkit and taxonomy of ai explainability techniques. *arXiv preprint arXiv:1909.03012*, 2019.
- [6] Barredo Arrieta, A., Díaz-Rodríguez, N., Del Ser, J., Bennetot, A., Tabik, S., Barbado, A., Garcia, S., Gil-Lopez, S., Molina, D., Benjamins, R., Chatila, R., and Herrera, F. Explainable artificial intelligence (xai): Concepts, taxonomies, opportunities and challenges toward responsible ai. *Inf. Fusion*, 58(C):82–115, jun 2020. ISSN 1566-2535. doi:10.1016/j.inffus.2019.12.012.
- [7] Batzner, S., Musaelian, A., Sun, L., Geiger, M., Mailoa, J. P., Kornbluth, M., Molinari, N., Smidt, T. E., and Kozinsky, B. E (3)-equivariant graph neural networks for data-efficient and accurate interatomic potentials. *Nature communications*, 13(1):1–11, 2022.
- [8] Bhatt, U., Weller, A., and Moura, J. M. Evaluating and aggregating feature-based model explanations. *arXiv preprint arXiv:2005.00631*, 2020.
- [9] Biscione, V. and Bowers, J. Learning translation invariance in cnns. *arXiv preprint arXiv:2011.11757*, 2020.
- [10] Bronstein, M. M., Bruna, J., Cohen, T., and Veličković, P. Geometric deep learning: Grids, groups, graphs, geodesics, and gauges. *arXiv preprint arXiv:2104.13478*, 2021.
- [11] Chawla, N. V., Bowyer, K. W., Hall, L. O., and Kegelmeyer, W. P. Smote: synthetic minority over-sampling technique. *Journal of artificial intelligence research*, 16:321–357, 2002.
- [12] Chen, C., Li, O., Tao, D., Barnett, A., Rudin, C., and Su, J. K. This looks like that: Deep learning for interpretable image recognition. In Wallach, H., Larochelle, H., Beygelzimer, A., d'Alché-Buc, F., Fox, E., and Garnett, R. (eds.), *Advances in Neural Information Processing Systems*, volume 32. Curran Associates, Inc., 2019.
- [13] Ching, T., Himmelstein, D. S., Beaulieu-Jones, B. K., Kalinin, A. A., Do, B. T., Way, G. P., Ferrero, E., Agapow, P.-M., Zietz, M., Hoffman, M. M., et al. Opportunities and obstacles for deep learning in biology and medicine. *Journal of The Royal Society Interface*, 15(141):20170387, 2018.
- [14] Choi, E., Bahadori, M. T., Sun, J., Kulas, J., Schuetz, A., and Stewart, W. Retain: An interpretable predictive model for healthcare using reverse time attention mechanism. *Advances in neural information processing systems*, 29, 2016.
- [15] Cohen, T. and Welling, M. Group equivariant convolutional networks. In Balcan, M. F. and Weinberger, K. Q. (eds.), *Proceedings of The 33rd International Conference on Machine Learning*, volume 48 of *Proceedings of Machine Learning Research*, pp. 2990–2999, New York, New York, USA, 2016. PMLR.
- [16] Cohen, T. S., Geiger, M., Köhler, J., and Welling, M. Spherical cnns. *arXiv preprint arXiv:1801.10130*, 2018.
- [17] Crabbé, J. and van der Schaar, M. Concept activation regions: A generalized framework for concept-based explanations. *arXiv preprint arXiv:2209.11222*, 2022.
- [18] Crabbe, J., Qian, Z., Imrie, F., and van der Schaar, M. Explaining latent representations with a corpus of examples. In Ranzato, M., Beygelzimer, A., Dauphin, Y., Liang, P., and Vaughan, J. W. (eds.), *Advances in Neural Information Processing Systems*, volume 34, pp. 12154–12166. Curran Associates, Inc., 2021.
- [19] Crabbé, J., Curth, A., Bica, I., and van der Schaar, M. Benchmarking heterogeneous treatment effect models through the lens of interpretability. *arXiv preprint arXiv:2206.08363*, 2022.
- [20] Dombrowski, A.-K., Alber, M., Anders, C., Ackermann, M., Müller, K.-R., and Kessel, P. Explanations can be manipulated and geometry is to blame. *Advances in Neural Information Processing Systems*, 32, 2019.
- [21] Doshi-Velez, F. and Kim, B. Towards a rigorous science of interpretable machine learning. *arXiv preprint arXiv:1702.08608*, 2017.

- [22] Erion, G., Janizek, J. D., Sturmfels, P., Lundberg, S. M., and Lee, S.-I. Improving performance of deep learning models with axiomatic attribution priors and expected gradients. *Nature machine intelligence*, 3(7):620–631, 2021.
- [23] Fey, M. and Lenssen, J. E. Fast graph representation learning with PyTorch Geometric. In *ICLR Workshop on Representation Learning on Graphs and Manifolds*, 2019.
- [24] Fisher, A., Rudin, C., and Dominici, F. All models are wrong, but many are useful: Learning a variable’s importance by studying an entire class of prediction models simultaneously. *J. Mach. Learn. Res.*, 20(177):1–81, 2019.
- [25] Garima, Liu, F., Kale, S., and Sundararajan, M. Estimating training data influence by tracing gradient descent. In *Proceedings of the 34th International Conference on Neural Information Processing Systems, NIPS’20*, Red Hook, NY, USA, 2020. Curran Associates Inc. ISBN 9781713829546.
- [26] Ghorbani, A., Abid, A., and Zou, J. Interpretation of neural networks is fragile. In *Proceedings of the AAAI conference on artificial intelligence*, volume 33, 2019.
- [27] Goldberger, A. L., Amaral, L. A., Glass, L., Hausdorff, J. M., Ivanov, P. C., Mark, R. G., Mietus, J. E., Moody, G. B., Peng, C. K., and Stanley, H. E. PhysioBank, PhysioToolkit, and PhysioNet: components of a new research resource for complex physiologic signals. *Circulation*, 101(23), 2000. ISSN 15244539. doi:10.1161/01.cir.101.23.e215.
- [28] Hagberg, A. A., Schult, D. A., and Swart, P. J. Exploring network structure, dynamics, and function using networkx. In Varoquaux, G., Vaught, T., and Millman, J. (eds.), *Proceedings of the 7th Python in Science Conference*, pp. 11 – 15, Pasadena, CA USA, 2008.
- [29] Hancox-Li, L. Robustness in machine learning explanations: Does it matter? In *Proceedings of the 2020 Conference on Fairness, Accountability, and Transparency, FAT\* ’20*, pp. 640–647, New York, NY, USA, 2020. Association for Computing Machinery. ISBN 9781450369367. doi:10.1145/3351095.3372836.
- [30] Hanocka, R., Hertz, A., Fish, N., Giryas, R., Fleishman, S., and Cohen-Or, D. Meshcnn: a network with an edge. *ACM Transactions on Graphics (TOG)*, 38(4):1–12, 2019.
- [31] Hoeffding, W. Probability inequalities for sums of bounded random variables. *Journal of the American Statistical Association*, 58(301):13–30, 1963. ISSN 01621459.
- [32] Huang, W., Zhao, X., Jin, G., and Huang, X. Safari: Versatile and efficient evaluations for robustness of interpretability. *arXiv preprint arXiv:2208.09418*, 2022.
- [33] Joshi, C. Transformers are graph neural networks. *The Gradient*, pp. 5, 2020.
- [34] Jumper, J., Evans, R., Pritzel, A., Green, T., Figurnov, M., Ronneberger, O., Tunyasuvunakool, K., Bates, R., Židek, A., Potapenko, A., et al. Highly accurate protein structure prediction with alphafold. *Nature*, 596(7873): 583–589, 2021.
- [35] Kachuee, M., Fazeli, S., and Sarrafzadeh, M. Ecg heartbeat classification: A deep transferable representation. In *2018 IEEE international conference on healthcare informatics (ICHI)*, pp. 443–444. IEEE, 2018.
- [36] Kayhan, O. S. and Gemert, J. C. v. On translation invariance in cnns: Convolutional layers can exploit absolute spatial location. In *Proceedings of the IEEE/CVF Conference on Computer Vision and Pattern Recognition*, pp. 14274–14285, 2020.
- [37] Kazius, J., McGuire, R., and Bursi, R. Derivation and validation of toxicophores for mutagenicity prediction. *Journal of Medicinal Chemistry*, 48(1):312–320, 2005. doi:10.1021/jm040835a. PMID: 15634026.
- [38] Keriven, N. and Peyré, G. Universal invariant and equivariant graph neural networks. *Advances in Neural Information Processing Systems*, 32, 2019.
- [39] Kim, B., Wattenberg, M., Gilmer, J., Cai, C., Wexler, J., Viegas, F., et al. Interpretability beyond feature attribution: Quantitative testing with concept activation vectors (tcav). In *International conference on machine learning*, pp. 2668–2677. PMLR, 2018.
- [40] Kindermans, P.-J., Hooker, S., Adebayo, J., Alber, M., Schütt, K. T., Dähne, S., Erhan, D., and Kim, B. The (un) reliability of saliency methods. In *Explainable AI: Interpreting, Explaining and Visualizing Deep Learning*, pp. 267–280. Springer, 2019.
- [41] Kingma, D. P. and Ba, J. Adam: A method for stochastic optimization. *arXiv preprint arXiv:1412.6980*, 2014.
- [42] Kloek, T. and van Dijk, H. K. Bayesian estimates of equation system parameters: An application of integration by monte carlo. *Econometrica*, 46(1):1–19, 1978. ISSN 00129682, 14680262.

- [43] Koh, P. W. and Liang, P. Understanding black-box predictions via influence functions. In Precup, D. and Teh, Y. W. (eds.), *Proceedings of the 34th International Conference on Machine Learning*, volume 70 of *Proceedings of Machine Learning Research*, pp. 1885–1894. PMLR, 2017.
- [44] Kokhlikyan, N., Miglani, V., Martin, M., Wang, E., Alsallakh, B., Reynolds, J., Melnikov, A., Kliushkina, N., Araya, C., Yan, S., and Reblitz-Richardson, O. Captum: A unified and generic model interpretability library for pytorch, 2020.
- [45] Lage, I., Chen, E., He, J., Narayanan, M., Kim, B., Gershman, S. J., and Doshi-Velez, F. Human evaluation of models built for interpretability. In *Proceedings of the AAAI Conference on Human Computation and Crowdsourcing*, volume 7, pp. 59–67, 2019.
- [46] Langer, M., Oster, D., Speith, T., Hermanns, H., Kästner, L., Schmidt, E., Sesing, A., and Baum, K. What do we want from explainable artificial intelligence (xai)?—a stakeholder perspective on xai and a conceptual model guiding interdisciplinary xai research. *Artificial Intelligence*, 296:103473, 2021.
- [47] Lee, J., Lee, Y., Kim, J., Kosiorek, A., Choi, S., and Teh, Y. W. Set transformer: A framework for attention-based permutation-invariant neural networks. In *International conference on machine learning*, pp. 3744–3753. PMLR, 2019.
- [48] Lipton, Z. C. The mythos of model interpretability: In machine learning, the concept of interpretability is both important and slippery. *Queue*, 16(3):31–57, 2018.
- [49] Lundberg, S. M. and Lee, S.-I. A unified approach to interpreting model predictions. In Guyon, I., Luxburg, U. V., Bengio, S., Wallach, H., Fergus, R., Vishwanathan, S., and Garnett, R. (eds.), *Advances in Neural Information Processing Systems*, volume 30. Curran Associates, Inc., 2017.
- [50] Moody, G. and Mark, R. The impact of the mit-bih arrhythmia database. *IEEE Engineering in Medicine and Biology Magazine*, 20(3):45–50, 2001. doi:10.1109/51.932724.
- [51] Morris, C., Ritzert, M., Fey, M., Hamilton, W. L., Lenssen, J. E., Rattan, G., and Grohe, M. Weisfeiler and leman go neural: Higher-order graph neural networks. In *Proceedings of the AAAI conference on artificial intelligence*, volume 33, pp. 4602–4609, 2019.
- [52] Morris, C., Kriege, N. M., Bause, F., Kersting, K., Mutzel, P., and Neumann, M. Tudataset: A collection of benchmark datasets for learning with graphs. In *ICML 2020 Workshop on Graph Representation Learning and Beyond (GRL+ 2020)*, 2020.
- [53] Nielsen, I. E., Dera, D., Rasool, G., Ramachandran, R. P., and Bouaynaya, N. C. Robust explainability: A tutorial on gradient-based attribution methods for deep neural networks. *IEEE Signal Processing Magazine*, 39(4):73–84, 2022. doi:10.1109/MSP.2022.3142719.
- [54] Paszke, A., Gross, S., Chintala, S., Chanan, G., Yang, E., DeVito, Z., Lin, Z., Desmaison, A., Antiga, L., and Lerer, A. Automatic differentiation in pytorch. *arXiv preprint*, 2017.
- [55] Pedregosa, F., Varoquaux, G., Gramfort, A., Michel, V., Thirion, B., Grisel, O., Blondel, M., Prettenhofer, P., Weiss, R., Dubourg, V., Vanderplas, J., Passos, A., Cournapeau, D., Brucher, M., Perrot, M., and Duchesnay, E. Scikit-learn: Machine learning in Python. *Journal of Machine Learning Research*, 12:2825–2830, 2011.
- [56] Ribeiro, M. T., Singh, S., and Guestrin, C. "why should i trust you?": Explaining the predictions of any classifier. In *Proceedings of the 22nd ACM SIGKDD International Conference on Knowledge Discovery and Data Mining*, KDD '16, pp. 1135–1144, New York, NY, USA, 2016. Association for Computing Machinery. ISBN 9781450342322. doi:10.1145/2939672.2939778.
- [57] Riesen, K. and Bunke, H. Iam graph database repository for graph based pattern recognition and machine learning. In *Joint IAPR International Workshops on Statistical Techniques in Pattern Recognition (SPR) and Structural and Syntactic Pattern Recognition (SSPR)*, pp. 287–297. Springer, 2008.
- [58] Robinson, D., Gehring, F., and Halmos, P. *A Course in the Theory of Groups*. Graduate Texts in Mathematics. Springer New York, 1996. ISBN 9780387944616.
- [59] Rudin, C. Stop explaining black box machine learning models for high stakes decisions and use interpretable models instead. *Nature Machine Intelligence*, 1(5):206–215, 2019.
- [60] Saporta, A., Gui, X., Agrawal, A., Pareek, A., Truong, S. Q., Nguyen, C. D., Ngo, V.-D., Seekins, J., Blankenberg, F. G., Ng, A. Y., et al. Benchmarking saliency methods for chest x-ray interpretation. *Nature Machine Intelligence*, pp. 1–12, 2022.
- [61] Satorras, V. G., Hoogeboom, E., and Welling, M. E(n) equivariant graph neural networks. In Meila, M. and Zhang, T. (eds.), *Proceedings of the 38th International Conference on Machine Learning*, volume 139 of *Proceedings of Machine Learning Research*, pp. 9323–9332. PMLR, 2021.

- [62] Shrikumar, A., Greenside, P., and Kundaje, A. Learning important features through propagating activation differences. In *International conference on machine learning*, pp. 3145–3153. PMLR, 2017.
- [63] Simonyan, K., Vedaldi, A., and Zisserman, A. Deep inside convolutional networks: Visualising image classification models and saliency maps. In Bengio, Y. and LeCun, Y. (eds.), *2nd International Conference on Learning Representations, ICLR 2014, Workshop Track Proceedings*, 2014.
- [64] Springenberg, J. T., Dosovitskiy, A., Brox, T., and Riedmiller, M. Striving for simplicity: The all convolutional net. *arXiv preprint arXiv:1412.6806*, 2014.
- [65] Sturmfels, P., Lundberg, S., and Lee, S.-I. Visualizing the impact of feature attribution baselines. *Distill*, 5(1):e22, 2020.
- [66] Sundararajan, M., Taly, A., and Yan, Q. Axiomatic attribution for deep networks. In *Proceedings of the 34th International Conference on Machine Learning - Volume 70, ICML'17*, pp. 3319–3328. JMLR.org, 2017.
- [67] Szegedy, C., Zaremba, W., Sutskever, I., Bruna, J., Erhan, D., Goodfellow, I. J., and Fergus, R. Intriguing properties of neural networks. In Bengio, Y. and LeCun, Y. (eds.), *2nd International Conference on Learning Representations, ICLR 2014, Banff, AB, Canada, April 14-16, 2014, Conference Track Proceedings*, 2014.
- [68] Tallec, C. and Ollivier, Y. Can recurrent neural networks warp time? *arXiv preprint arXiv:1804.11188*, 2018.
- [69] Van Rossum, G. and Drake, F. L. *Python 3 Reference Manual*. CreateSpace, Scotts Valley, CA, 2009. ISBN 1441412697.
- [70] Vaswani, A., Shazeer, N., Parmar, N., Uszkoreit, J., Jones, L., Gomez, A. N., Kaiser, L. u., and Polosukhin, I. Attention is all you need. In Guyon, I., Luxburg, U. V., Bengio, S., Wallach, H., Fergus, R., Vishwanathan, S., and Garnett, R. (eds.), *Advances in Neural Information Processing Systems*, volume 30. Curran Associates, Inc., 2017.
- [71] Wang, Y. and Wang, X. Self-interpretable model with transformation equivariant interpretation. *Advances in Neural Information Processing Systems*, 34:2359–2372, 2021.
- [72] Wang, Z., Wang, H., Ramkumar, S., Mardziel, P., Fredrikson, M., and Datta, A. Smoothed geometry for robust attribution. *Advances in Neural Information Processing Systems*, 33:13623–13634, 2020.
- [73] Wu, Z., Song, S., Khosla, A., Yu, F., Zhang, L., Tang, X., and Xiao, J. 3d shapenets: A deep representation for volumetric shapes. In *2015 IEEE Conference on Computer Vision and Pattern Recognition (CVPR)*, pp. 1912–1920, 2015. doi:10.1109/CVPR.2015.7298801.
- [74] Wu, Z., Pan, S., Chen, F., Long, G., Zhang, C., and Philip, S. Y. A comprehensive survey on graph neural networks. *IEEE transactions on neural networks and learning systems*, 32(1):4–24, 2020.
- [75] Xie, S., Girshick, R., Dollár, P., Tu, Z., and He, K. Aggregated residual transformations for deep neural networks. In *Proceedings of the IEEE conference on computer vision and pattern recognition*, pp. 1492–1500, 2017.
- [76] Xie, Y., Vosoughi, S., and Hassanpour, S. Interpretation quality score for measuring the quality of interpretability methods. *arXiv preprint arXiv:2205.12254*, 2022.
- [77] Yeh, C.-K., Hsieh, C.-Y., Suggala, A., Inouye, D. I., and Ravikumar, P. K. On the (in) fidelity and sensitivity of explanations. *Advances in Neural Information Processing Systems*, 32, 2019.
- [78] Zaheer, M., Kottur, S., Ravanbakhsh, S., Póczos, B., Salakhutdinov, R. R., and Smola, A. J. Deep sets. *Advances in neural information processing systems*, 30, 2017.
- [79] Zeiler, M. D. and Fergus, R. Visualizing and understanding convolutional networks. In *European conference on computer vision*, pp. 818–833. Springer, 2014.
- [80] Zhou, J., Gandomi, A. H., Chen, F., and Holzinger, A. Evaluating the quality of machine learning explanations: A survey on methods and metrics. *Electronics*, 10(5):593, 2021.

## A Guidelines Flowchart

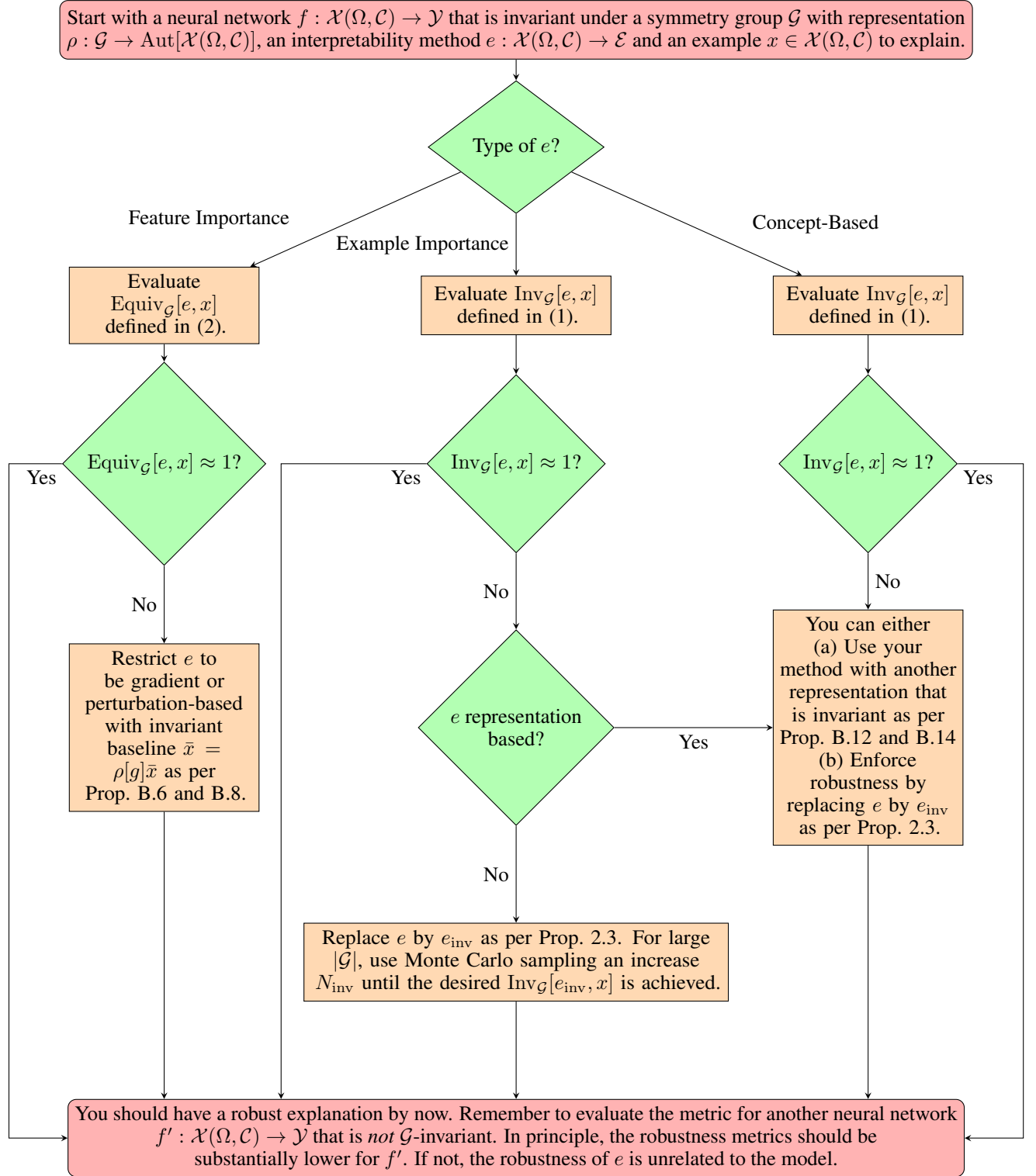


Figure 5: Our guideline to improve the robustness of interpretability methods with respect to model symmetries.



## B Theoretical Results

In this appendix, we prove all the theoretical results mentioned in the main paper. We start by deriving robustness guarantees mentioned in Table 1. We then prove that any method can be made  $\mathcal{G}$ -invariant by aggregating the explanation over several symmetries.

### B.1 Feature Importance Guarantees

Let us start by feature importance methods. As we are going to see, the robustness guarantees in this case typically require us to restrict the type of group representation  $\rho$  we use to encode the action of the symmetry group  $\mathcal{G}$  on the signal space  $\mathcal{X}(\Omega, \mathcal{C})$ . This motivates the two following types of representations that can be found in group theory textbooks (see e.g. [58]).

**Definition B.1** (Orthogonal Representation). Let  $\rho : \mathcal{G} \rightarrow \text{Aut}[\mathcal{X}(\Omega, \mathcal{C})]$  be a representation of the group  $\mathcal{G}$ , and let  $d \in \mathbb{N}^+$  denote the dimension of the signal space  $\mathcal{X}(\Omega, \mathcal{C})$ . We say that the representation is an *orthogonal representation* if its image is a subset on the orthogonal matrices acting on  $\mathcal{X}(\Omega, \mathcal{C})$ :  $\rho(\mathcal{G}) \subseteq O(d)$ , where  $O(d)$  denotes the set of  $d \times d$  orthogonal real matrices. This is equivalent to  $\rho[g]\rho^\top[g] = \rho^\top[g]\rho[g] = I_d$  for all  $g \in \mathcal{G}$ , where  $I_d$  denotes the  $d \times d$  identity matrix.

**Definition B.2** (Permutation Representation). Let  $\rho : \mathcal{G} \rightarrow \text{Aut}[\mathcal{X}(\Omega, \mathcal{C})]$  be a representation of the group  $\mathcal{G}$ , and let  $d \in \mathbb{N}^+$  denote the dimension of the signal space  $\mathcal{X}(\Omega, \mathcal{C})$ . We say that the representation is a *permutation representation* if its image is a subset on the permutation matrices acting on  $\mathcal{X}(\Omega, \mathcal{C})$ :  $\rho(\mathcal{G}) \subseteq P(d)$ , where  $P(d)$  denotes the set of  $d \times d$  permutation matrices. This means that for all  $g \in \mathcal{G}$ , there exists some permutation  $\pi \in S(d)$  such that we can write  $(\rho[g]x)_i = x_{\pi(i)}$  for all  $i \in \mathbb{Z}_d, x \in \mathcal{X}(\Omega, \mathcal{C})$ .

*Remark B.3.* One can easily check that all permutation representations are also orthogonal representations. The opposite is not true.

#### B.1.1 Gradient-Based

We shall now begin with gradient-based feature importance methods. These methods compute the model's gradient with respect to the input features to compute the importance scores. Hence, it is useful to characterize how this gradient transforms under the action of the symmetry group  $\mathcal{G}$ .

**Lemma B.4** (Gradient Transformation). *Consider a differentiable function  $f : \mathcal{X}(\Omega, \mathcal{C}) \rightarrow \mathcal{Y}$  that is invariant with respect to the symmetry group  $\mathcal{G}$ . We assume that  $\mathcal{G}$  acts on  $\mathcal{X}(\Omega, \mathcal{C})$  via the representation  $\rho : \mathcal{G} \rightarrow \text{Aut}[\mathcal{X}(\Omega, \mathcal{C})]$ . If for some  $g \in \mathcal{G}$  we define  $x' = \rho[g]x$ , then we have the following identity:*

$$\nabla_{x'} f(x') = \rho^{-1, \top}[g] \nabla_x f(x), \quad (3)$$

where  $\rho^{-1, \top}[g]$  denotes the matrix obtained by applying an inversion followed by a transposition to the matrix  $\rho[g]$ .

*Proof.* We start by noting that the  $\mathcal{G}$ -invariance of  $f$  implies that  $f(x') = f(x)$  and, hence:

$$\nabla_{x'} f(x') = \nabla_x f(x) \quad (4)$$

It remains to establish the link between  $\nabla_{x'}$  and  $\nabla_x$ . To this end, we simply note that  $x = \rho^{-1}[g]x'$ . Hence, for all  $i \in \mathbb{Z}_d$  with  $d = \dim[\mathcal{X}(\Omega, \mathcal{C})]$ , we have that

$$x_i = \sum_{j=1}^d \rho_{ij}^{-1}[g] x'_j.$$

Hence, by using the chain rule, we deduce that for all  $k \in \mathbb{Z}_d$ :

$$\begin{aligned} \frac{\partial}{\partial x'_k} &= \sum_{i=1}^d \frac{\partial x_i}{\partial x'_k} \frac{\partial}{\partial x_i} \\ &= \sum_{i=1}^d \rho_{ik}^{-1}[g] \frac{\partial}{\partial x_i} \\ &= \sum_{i=1}^d \rho_{ki}^{-1, \top}[g] \frac{\partial}{\partial x_i}. \end{aligned}$$

The above identity implies  $\nabla_{x'} = \rho^{-1, \top}[g] \nabla_x$ . By injecting this to the right-hand side of (4), we obtain (3).  $\square$

The simplest gradient-based attribution is simply given by the gradient itself [63]. We refer to it as the vanilla saliency feature importance. Although this attribution method is a bit naive, we may still deduce an equivariance guarantee from the previous proposition.

**Corollary B.5** (Equivariance of Vanilla Saliency). *Consider a differentiable neural network  $f : \mathcal{X}(\Omega, \mathcal{C}) \rightarrow \mathcal{Y}$  that is invariant with respect to the symmetry group  $\mathcal{G}$ . We assume that  $\mathcal{G}$  acts on  $\mathcal{X}(\Omega, \mathcal{C})$  via the representation  $\rho : \mathcal{G} \rightarrow \text{Aut}[\mathcal{X}(\Omega, \mathcal{C})]$ . We consider a vanilla saliency feature importance explanation  $e(x) = \nabla_x f(x)$ . If the representation  $\rho$  is orthogonal, then the explanation  $e$  is  $\mathcal{G}$ -equivariant.*

*Proof.* From Lemma B.4, we have that  $e(\rho[g]x) = \rho^{-1, \top}[g]e(x)$  for all  $g \in \mathcal{G}$ . Now if  $\rho$  is orthogonal, we note that  $\rho^{-1, \top}[g] = \rho[g]$ , which proves the proposition.  $\square$

We now turn to a more general family of gradient-based feature importance methods. These methods attribute importance to each feature by aggregating gradients over a line in the input space  $\mathcal{X}(\Omega, \mathcal{C})$  connecting a baseline example  $\bar{x} \in \mathcal{X}(\Omega, \mathcal{C})$  with the example  $x \in \mathcal{X}(\Omega, \mathcal{C})$  we wish to explain. It was shown that the choice of this baseline signal has a significant impact on the resulting explanation [65]. In the following proposition, we show that enforcing equivariance imposes a restriction on the type of baseline signal  $\bar{x}$  that can be used in practice.

**Proposition B.6** (Gradient-Based Equivariance). *Consider a differentiable neural network  $f : \mathcal{X}(\Omega, \mathcal{C}) \rightarrow \mathcal{Y}$  that is invariant with respect to the symmetry group  $\mathcal{G}$ . We assume that  $\mathcal{G}$  acts on  $\mathcal{X}(\Omega, \mathcal{C})$  via the representation  $\rho : \mathcal{G} \rightarrow \text{Aut}[\mathcal{X}(\Omega, \mathcal{C})]$ . We consider a gradient-based explanation built upon a baseline signal  $\bar{x} \in \mathcal{X}(\Omega, \mathcal{C})$  and of the form*

$$e(x) = (x - \bar{x}) \odot \int_0^1 \varphi(t) \nabla_x f([\bar{x} + t(x - \bar{x})]) dt,$$

where  $\odot$  denotes the Hadamard product and  $\varphi$  is a functional defined on the Hilbert space  $L^2([0, 1])$ . If  $\rho$  is a permutation representation and the baseline signal is  $\mathcal{G}$ -invariant, i.e.  $\rho[g]\bar{x} = \bar{x}$  for all  $g \in \mathcal{G}$ , then the explanation  $e$  is  $\mathcal{G}$ -equivariant.

*Remark B.7.* Note that we have introduced the functional  $\varphi$  to make the class of explanation as general as possible. For instance, we obtain exact Integrated Gradients for  $\varphi(t) = 1$  and Input\*Gradient [62] for  $\varphi(t) = \delta(t - 1)$ , where  $\delta$  is a Dirac delta distribution. Similarly, this includes discrete approximations of Integrated Gradients by taking e.g.  $\varphi(t) = \sum_{n=1}^N \delta(t - t_n)$ , with  $t_n = \bar{x} + \frac{n}{N}(x - \bar{x})$  for all  $n \in \mathbb{Z}_N$ . Finally, we note that the equivariance of Integrated Gradients also implies the equivariance of Expected Gradients [22].

*Proof.* For all  $g \in \mathcal{G}$ , we have that:

$$\begin{aligned} e(\rho[g]x) &= (\rho[g]x - \bar{x}) \odot \int_0^1 \varphi(t) \nabla_x f(\bar{x} + t[\rho[g]x - \bar{x}]) dt \\ &= \rho[g](x - \bar{x}) \odot \int_0^1 \varphi(t) \nabla_x f(\rho[g][\bar{x} + t(x - \bar{x})]) dt && \text{(Invariance of } \bar{x} \text{)} \\ &= \rho[g](x - \bar{x}) \odot \rho[g] \int_0^1 \varphi(t) \nabla_x f(\bar{x} + t[x - \bar{x}]) dt && \text{(Corollary B.5).} \end{aligned}$$

Since  $\rho$  is a permutation representation, there exists a permutation  $\pi \in S(d)$ , where  $d = \dim[\mathcal{X}(\Omega, \mathcal{C})]$ , such that for all  $a, b \in \mathcal{X}(\Omega, \mathcal{C})$  and  $i \in \mathbb{Z}_d$ :

$$\begin{aligned} (\rho[g]a \odot \rho[g]b)_i &= (\rho[g]a)_i \odot (\rho[g]b)_i && \text{(Definition of Hadamard product)} \\ &= a_{\pi(i)} \odot b_{\pi(i)} && (\rho \text{ is a permutation representation)} \\ &= (a \odot b)_{\pi(i)} && \text{(Definition of Hadamard product)} \\ &= (\rho[g](a \odot b))_i && (\rho \text{ is a permutation representation).} \end{aligned}$$

We deduce that  $\rho[g]a \odot \rho[g]b = \rho[g](a \odot b)$ . By applying this to the above equation for  $e(\rho[g]x)$ , we get:

$$\begin{aligned} e(\rho[g]x) &= \rho[g](x - \bar{x}) \odot \rho[g] \int_0^1 \varphi(t) \nabla_x f(\bar{x} + t[x - \bar{x}]) dt \\ &= \rho[g] \left( (x - \bar{x}) \odot \int_0^1 \varphi(t) \nabla_x f(\bar{x} + t[x - \bar{x}]) dt \right) \\ &= \rho[g]e(x), \end{aligned}$$

which proves the equivariance property.  $\square$

### B.1.2 Perturbation-Based

The second type of feature importance methods we consider are perturbation-based methods. These methods attribute importance to each feature by measuring the impact of replacing some features of the example  $x \in \mathcal{X}(\Omega, \mathcal{C})$  with features from a baseline example  $\bar{x} \in \mathcal{X}(\Omega, \mathcal{C})$  on the model's prediction. Again, enforcing equivariance imposes a restriction on the type of baseline that can be manipulated.

**Proposition B.8** (Perturbation-Based Equivariance). *Consider a neural network  $f : \mathcal{X}(\Omega, \mathcal{C}) \rightarrow \mathcal{Y}$  that is invariant with respect to the symmetry group  $\mathcal{G}$ . We assume that  $\mathcal{G}$  acts on  $\mathcal{X}(\Omega, \mathcal{C})$  via the representation  $\rho : \mathcal{G} \rightarrow \text{Aut}[\mathcal{X}(\Omega, \mathcal{C})]$ . We consider a perturbation-based explanation built upon a baseline signal  $\bar{x} \in \mathcal{X}(\Omega, \mathcal{C})$  and of the form*

$$[e(x)]_i = f(x) - f(r_i(x)),$$

for all  $i \in \mathbb{Z}_d$ , where  $d = \dim[\mathcal{X}(\Omega, \mathcal{C})]$ . The perturbation operator  $r_i$  replaces feature  $x_i, i \in \mathbb{Z}_d$  with the baseline feature  $\bar{x}_i$ . It is defined as follows:  $[r_i(x)]_j = x_j + \delta_{ij}(\bar{x}_i - x_i)$ , where  $\delta$  denotes the Kronecker delta symbol, for all  $j \in \mathbb{Z}_d$  and  $x \in \mathcal{X}(\Omega, \mathcal{C})$ . If  $\rho$  is a permutation representation and the baseline signal is  $\mathcal{G}$ -invariant, i.e.  $\rho[g]\bar{x} = \bar{x}$  for all  $g \in \mathcal{G}$ , then the explanation  $e$  is  $\mathcal{G}$ -equivariant.

*Proof.* For all  $g \in \mathcal{G}$  and  $i, j \in \mathbb{Z}_d$ , there exists a permutation  $\pi \in S(d)$  such that:

$$\begin{aligned} [r_i(\rho[g]x)]_j &= x_{\pi(j)} + \delta_{ij}(\bar{x}_i - x_{\pi(i)}) && (\rho \text{ is a permutation representation}) \\ &= x_{\pi(j)} + \delta_{ij}(\bar{x}_{\pi(i)} - x_{\pi(i)}) && (\bar{x} \text{ is invariant}) \\ &= [r_{\pi(i)}(x)]_{\pi(j)} \\ &= [\rho[g]r_{\pi(i)}(x)]_j && (\rho \text{ is a permutation representation}). \end{aligned}$$

We deduce that  $r_i(\rho[g]x) = \rho[g]r_{\pi(i)}(x)$  for all  $i \in \mathbb{Z}_d$ . We are now ready to conclude as:

$$\begin{aligned} [e(\rho[g]x)]_i &= f(x) - f(r_i(\rho[g]x)) && (\text{Definition of } e) \\ &= f(x) - f(\rho[g]r_{\pi(i)}(x)) && (\text{Above identity}) \\ &= f(x) - f(r_{\pi(i)}(x)) && (\text{Invariance of } f) \\ &= [e(x)]_{\pi(i)} && (\text{Definition of } e) \\ &= [\rho[g]e(x)]_i && (\rho \text{ is a permutation representation}), \end{aligned}$$

which proves the equivariance property. □

## B.2 Example Importance Guarantees

We proceed with example importance methods.

### B.2.1 Loss-Based

We start with loss-based methods. These methods attribute importance to each training example of  $(x^n, y^n) \in \mathcal{D}_{\text{train}}$  by comparing the loss  $\mathcal{L}(f(x^n), y^n)$  with the loss  $\mathcal{L}(f(x), y)$  of the example  $x \in \mathcal{X}(\Omega, \mathcal{C})$  we wish to explain. We show that these methods are naturally invariant without imposing any restriction on the representation  $\rho$ .

**Proposition B.9** (Loss-Based Invariance). *Consider a differentiable neural network  $f_\theta : \mathcal{X}(\Omega, \mathcal{C}) \rightarrow \mathcal{Y}$ , parametrized by  $P \in \mathbb{N}^+$  parameters  $\theta \in \mathbb{R}^P$ , that is invariant with respect to the symmetry group  $\mathcal{G}$ . We assume that  $\mathcal{G}$  acts on  $\mathcal{X}(\Omega, \mathcal{C})$  via the representation  $\rho : \mathcal{G} \rightarrow \text{Aut}[\mathcal{X}(\Omega, \mathcal{C})]$ . We consider an example importance explanation based on the loss  $\mathcal{L} : \mathcal{X}(\Omega, \mathcal{C}) \times \mathcal{Y} \rightarrow \mathbb{R}^+$  and of the form*

$$e(x, y) = \mathcal{F}[\mathcal{L}(f_\theta(x), y)],$$

where  $\mathcal{F}$  maps any function  $l : \mathbb{R}^P \rightarrow \mathbb{R}^+$  to a vector in  $\mathcal{F}[l] \in \mathbb{R}^{N_{\text{train}}}$ , with  $N_{\text{train}} \in \mathbb{N}^+$  corresponding to the number of training examples for which we evaluate the importance. The explanation  $e$  is  $\mathcal{G}$ -invariant.

*Remark B.10.* We note that  $\mathcal{F}$  typically contains differential operators. For instance, Influence Functions are obtained by taking

$$(\mathcal{F}[l])_n = \nabla_\theta^\top \mathcal{L}(f_\theta(x^n), y^n) H_\theta^{-1} \nabla_\theta l(\theta),$$

for  $n \in \mathbb{Z}_{N_{\text{train}}}$ , where  $(x^n, y^n) \in \mathcal{D}_{\text{train}}$  is a training example and  $H_\theta \in \mathbb{R}^{P \times P}$  is the Hessian of the training loss with respect to the model's parameters.

*Remark B.11.* We note that the dependency of the explanation  $e$  with respect to the label  $y \in \mathcal{Y}$  is omitted in the main paper. The reason for this is that the symmetry group  $\mathcal{G}$  only acts on the input signal  $x$ .

*Proof.* The proposition can directly be deduced from the  $\mathcal{G}$ -invariance of the model. For any  $g \in \mathcal{G}$ , we have:

$$\begin{aligned} e(\rho[g]x, y) &= \mathcal{F}[\mathcal{L}(f_\theta(\rho[g]x), y)] \\ &= \mathcal{F}[\mathcal{L}(f_\theta(x), y)] && \text{(Invariance of } f) \\ &= e(x, y), \end{aligned}$$

which proves the desired property.  $\square$

## B.2.2 Representation-Based

We proceed with representation-based methods. These methods attribute importance to each training example of  $(x^n, y^n) \in \mathcal{D}_{\text{train}}$  by comparing the model's representation  $h(x^n)$  (typically the output of a model's layer) with the representation  $h(x)$  of the example  $x \in \mathcal{X}(\Omega, \mathcal{C})$  we wish to explain. We show that these methods are invariant if we restrict to representations  $h$  that are invariant.

**Proposition B.12** (Representation-Based Invariance). *Consider a differentiable neural network  $f : \mathcal{X}(\Omega, \mathcal{C}) \rightarrow \mathcal{Y}$  that is invariant with respect to the symmetry group  $\mathcal{G}$ . We assume that  $\mathcal{G}$  acts on  $\mathcal{X}(\Omega, \mathcal{C})$  via the representation  $\rho : \mathcal{G} \rightarrow \text{Aut}[\mathcal{X}(\Omega, \mathcal{C})]$ . We consider an example importance explanation based on a representation  $h : \mathcal{X}(\Omega, \mathcal{C}) \rightarrow \mathcal{H}$  extracted from  $f$  (e.g. an intermediate layer of the neural network) and of the form*

$$e(x) = \mathcal{F}[h(x)],$$

where  $\mathcal{F} : \mathcal{H} \rightarrow \mathbb{R}^{N_{\text{train}}}$  maps any representation  $r \in \mathcal{H}$  to a vector in  $\mathcal{F}[r] \in \mathbb{R}^{N_{\text{train}}}$ , with  $N_{\text{train}} \in \mathbb{N}^+$  corresponding to the number of training examples for which we evaluate the importance. If the representation  $h$  is  $\mathcal{G}$ -invariant, then the explanation  $e$  is  $\mathcal{G}$ -invariant.

*Remark B.13.* We note that  $\mathcal{F}$  can be adapted to the method we want to describe. For instance, SimpleX is obtained by taking

$$\begin{aligned} \mathcal{F}[r] &= \arg \min_{w \in [0,1]^{N_{\text{train}}}} \left[ r - \sum_{n=1}^{N_{\text{train}}} w_n h(x^n) \right] \\ \text{s.t. } &\sum_{n=1}^{N_{\text{train}}} w_n = 1 \end{aligned}$$

where  $x^n \in \mathcal{D}_{\text{train}}$  is a training example for  $n \in \mathbb{Z}_{N_{\text{train}}}$ . Similarly, Representation Similarity is obtained with

$$\mathcal{F}[r]_n = r^\top h(x^n),$$

for all  $n \in \mathbb{Z}_{N_{\text{train}}}$ .

*Proof.* The proposition can directly be deduced from the  $\mathcal{G}$ -invariance of the representation. For any  $g \in \mathcal{G}$ , we have:

$$\begin{aligned} e(\rho[g]x) &= \mathcal{F}[h(\rho[g]x)] \\ &= \mathcal{F}[h(x)] && \text{(Invariance of } h) \\ &= e(x), \end{aligned}$$

which proves the desired property.  $\square$

## B.3 Concept-Based Explanations Guarantees

We now turn to concept-based methods. These methods attribute importance to a set of concept specified by the user for the model to predict a certain class. Although these explanations are typically global (i.e. at the dataset level), they are based on concept classifiers that attempt to detect the presence/absence of the concept on each individual example  $x \in \mathcal{X}(\Omega, \mathcal{C})$  based on its representation  $h(x)$ . We show that these classifiers are  $\mathcal{G}$ -invariant if we restrict to representations  $h$  that are  $\mathcal{G}$ -invariant.

**Proposition B.14** (Concept-Based Invariance). *Consider a differentiable neural network  $f : \mathcal{X}(\Omega, \mathcal{C}) \rightarrow \mathcal{Y}$  that is invariant with respect to the symmetry group  $\mathcal{G}$ . We assume that  $\mathcal{G}$  acts on  $\mathcal{X}(\Omega, \mathcal{C})$  via the representation  $\rho : \mathcal{G} \rightarrow \text{Aut}[\mathcal{X}(\Omega, \mathcal{C})]$ . We consider a concept-based explanation based on a representation  $h : \mathcal{X}(\Omega, \mathcal{C}) \rightarrow \mathcal{H}$  extracted from  $f$  (e.g. an intermediate layer of the neural network) and of the form*

$$e(x) = c[h(x)],$$

where  $c : \mathcal{H} \rightarrow \{0, 1\}^C$  maps any representation  $r \in \mathcal{H}$  to a binary vector in  $c[r] \in \{0, 1\}^C$  indicating the presence/absence of  $C \in \mathbb{N}^+$  selected concepts. If the representation  $h$  is  $\mathcal{G}$ -invariant, then the explanation  $e$  is  $\mathcal{G}$ -invariant.

*Remark B.15.* We note that concepts activation vectors (CAVs) are obtained by fitting a linear classifier  $c$ . Concept activations regions (CARs), on the other hand, are obtained by fitting a kernel-based concept classifier.

*Proof.* The proposition can directly be deduced from the  $\mathcal{G}$ -invariance of the representation. For any  $g \in \mathcal{G}$ , we have:

$$\begin{aligned} e(\rho[g]x) &= c[h(\rho[g]x)] \\ &= c[h(x)] && \text{(Invariance of } h) \\ &= e(x), \end{aligned}$$

which proves the desired property.  $\square$

#### B.4 Enforcing Invariance

Finally, we prove Proposition 2.3 that allows us to turn any interpretability method into a  $\mathcal{G}$ -invariant method.

**Proposition B.16.** [*Enforce Invariance*] *Consider a neural network  $f : \mathcal{X}(\Omega, \mathcal{C}) \rightarrow \mathcal{Y}$  that is invariant with respect to the symmetry group  $\mathcal{G}$  and  $e : \mathcal{X}(\Omega, \mathcal{C}) \rightarrow \mathcal{E}$  be an explanation for  $f$ . We assume that  $\mathcal{G}$  acts on  $\mathcal{X}(\Omega, \mathcal{C})$  via the representation  $\rho : \mathcal{G} \rightarrow \text{Aut}[\mathcal{X}(\Omega, \mathcal{C})]$ . We define the auxiliary explanation  $e_{\text{inv}} : \mathcal{X}(\Omega, \mathcal{C}) \rightarrow \mathcal{E}$  as*

$$e_{\text{inv}}(x) \equiv \frac{1}{|\mathcal{G}|} \sum_{g \in \mathcal{G}} e(\rho[g]x)$$

for all  $x \in \mathcal{X}(\Omega, \mathcal{C})$ . The auxiliary explanation  $e_{\text{inv}}$  is invariant under the symmetry group  $\mathcal{G}$ .

*Proof.* For any  $\tilde{g} \in \mathcal{G}$ , we have that

$$\begin{aligned} e_{\text{inv}}(\rho[\tilde{g}]x) &= \frac{1}{|\mathcal{G}|} \sum_{g \in \mathcal{G}} e(\rho[\tilde{g}]\rho[g]x) \\ &= \frac{1}{|\mathcal{G}|} \sum_{g \in \mathcal{G}} e(\rho[\tilde{g} \circ g]x), \end{aligned}$$

where we have used the fact that the representation  $\rho$  is compatible with the group composition. We now define the map  $l_{\tilde{g}} : \mathcal{G} \rightarrow \mathcal{G}$  as  $l_{\tilde{g}}(g) = \tilde{g} \circ g$  for all  $g \in \mathcal{G}$ . We note that  $l_{\tilde{g}}$  is a bijection from  $\mathcal{G}$  to itself, since it admits an inverse  $l_{\tilde{g}}^{-1} = l_{\tilde{g}^{-1}}$ . Indeed, for all  $g \in \mathcal{G}$ :

$$\begin{aligned} (l_{\tilde{g}^{-1}} \circ l_{\tilde{g}})(g) &= \tilde{g}^{-1} \circ \tilde{g} \circ g = g \\ (l_{\tilde{g}} \circ l_{\tilde{g}^{-1}})(g) &= \tilde{g} \circ \tilde{g}^{-1} \circ g = g \end{aligned}$$

Hence, we have that  $l_{\tilde{g}}(\mathcal{G}) = \mathcal{G}$ . By denoting  $g' = l_{\tilde{g}}(g) = \tilde{g} \circ g$ , we can therefore write

$$\begin{aligned} e_{\text{inv}}(\rho[\tilde{g}]x) &= \sum_{g' \in \mathcal{G}} e(\rho[g']x) \\ &= e_{\text{inv}}(x). \end{aligned}$$

This proves the  $\mathcal{G}$ -invariance of the explanation  $e_{\text{inv}}$ .  $\square$

## C Convergence of the Monte Carlo Estimators

In this appendix, we discuss the Monte Carlo estimators used to approximate the invariance and equivariance metrics defined in Definition 2.1. We first note that our experiments typically aggregate the metrics over a test set  $\mathcal{D}_{\text{test}}$  of examples. Hence, we are interested in the metrics

$$\begin{aligned}\overline{\text{Inv}}_{\mathcal{G}}(e) &= \mathbb{E}_{X \sim U(\mathcal{D}_{\text{test}}), G \sim U(\mathcal{G})} [s_{\mathcal{E}} [e(\rho[G]X), e(X)]] \\ \overline{\text{Equiv}}_{\mathcal{G}}(e) &= \mathbb{E}_{X \sim U(\mathcal{D}_{\text{test}}), G \sim U(\mathcal{G})} [s_{\mathcal{E}} [e(\rho[G]X), \rho'[G]e(X)]] ,\end{aligned}$$

where  $U$  denotes a uniform distribution. Clearly, whenever the order  $|\mathcal{G}|$  of the symmetry group is large, these metrics might become prohibitively expensive to compute. In this setting, we simply build a Monte Carlo estimator for the above metrics by sampling  $N_{\text{samp}}$  symmetries  $G_1, \dots, G_{N_{\text{samp}}}$  with  $N_{\text{samp}} \in \mathbb{N}^+$  and  $N_{\text{samp}} \ll |\mathcal{G}|$ . If we have  $N_{\text{test}} = |\mathcal{D}_{\text{test}}|$  test examples, the Monte Carlo estimators can be written as

$$\begin{aligned}\widehat{\text{Inv}}_{\mathcal{G}}(e) &= \frac{1}{N_{\text{test}}N_{\text{samp}}} \sum_{n=1}^{N_{\text{test}}} \sum_{m=1}^{N_{\text{samp}}} s_{\mathcal{E}} [e(\rho[G_m]X^n), e(X^n)] \\ \widehat{\text{Equiv}}_{\mathcal{G}}(e) &= \frac{1}{N_{\text{test}}N_{\text{samp}}} \sum_{n=1}^{N_{\text{test}}} \sum_{m=1}^{N_{\text{samp}}} s_{\mathcal{E}} [e(\rho[G_m]X^n), \rho'[G_m]e(X^n)] .\end{aligned}$$

Those are the estimators that we use in our experiments. Let us first discuss the convergence of these estimators theoretically. Since  $s_{\mathcal{E}}(a, b) \in [-1, 1]$  for all  $a, b \in \mathcal{E}$ , Hoeffding [31]’s inequality guarantees that for all  $t \in \mathbb{R}^+$ :

$$\begin{aligned}\mathbb{P} \left( \left| \widehat{\text{Inv}}_{\mathcal{G}}(e) - \overline{\text{Inv}}_{\mathcal{G}}(e) \right| \geq t \right) &\leq 2 \exp \left( -\frac{N_{\text{test}}N_{\text{samp}}t^2}{2} \right) \\ \mathbb{P} \left( \left| \widehat{\text{Equiv}}_{\mathcal{G}}(e) - \overline{\text{Equiv}}_{\mathcal{G}}(e) \right| \geq t \right) &\leq 2 \exp \left( -\frac{N_{\text{test}}N_{\text{samp}}t^2}{2} \right) .\end{aligned}$$

Let us now plug-in some numbers to see how these inequalities translate in our experiments. In Section 3, we typically use  $N_{\text{test}} = 1,000$  and  $N_{\text{samp}} = 50$ . Hence, the probability of making an error larger than  $t = 2\%$  in our experiments is smaller than  $10^{-4}$ . This guarantees that all the metrics reported in the main paper are precisely evaluated.

We shall now verify this theoretical analysis with the experimental setup described in Section 3. Since we do not resort to any Monte Carlo approximation for the Electrocardiogram dataset, we exclude it from our analysis. Similarly, robustness scores  $\widehat{\text{Inv}}_{\mathcal{G}}(e) \approx 1$  or  $\widehat{\text{Equiv}}_{\mathcal{G}}(e) \approx 1$  can be excluded as these can only be produced by having  $\text{Inv}[e, G_m] \approx 1$  or  $\text{Equiv}[e, G_m] \approx 1$  for all  $m \in \mathbb{Z}_{N_{\text{samp}}}$ , which guarantees that the estimators have already converged. By applying these filters with the help of Figure 2, we restrict our analysis to Gradient Shap for the Mutagenicity dataset and to Gradient Shap, Feature Permutation, Simplex-Equiv, CAV-Equiv and CAR-Equiv for the ModelNet40 dataset. We plot the Monte Carlo estimators  $\widehat{\text{Inv}}_{\mathcal{G}}(e)$  and  $\widehat{\text{Equiv}}_{\mathcal{G}}(e)$  as a function of  $N_{\text{samp}}$  for various interpretability methods in Figure 6. As we can see, all the Monte Carlo estimators have already converged for  $N_{\text{samp}} = 50$  used in the experiment. This is due to the fact that we use a relatively large test set in each experiment, with  $N_{\text{test}} = 433$  for the Mutagenicity dataset and  $N_{\text{test}} = 1,000$  for the ModelNet40 experiment.

We finish this appendix by mentioning that all the groups manipulated in this paper are finite groups. It goes without saying that an extension of our analysis to infinite, or even uncountable groups would probably require a more sophisticated sampling technique, such as e.g. importance sampling [42].

## D Experiment Details

In this appendix, we provide all the details for the experiments conducted in Section 3.

**Computing Resources.** All the empirical evaluations were run on a single machine equipped with a 64-Core AMD Ryzen Threadripper PRO 3995WX CPU and a NVIDIA RTX A4000 GPU. The machine runs on Python 3.10 [69] and Pytorch 1.13.1 [54].

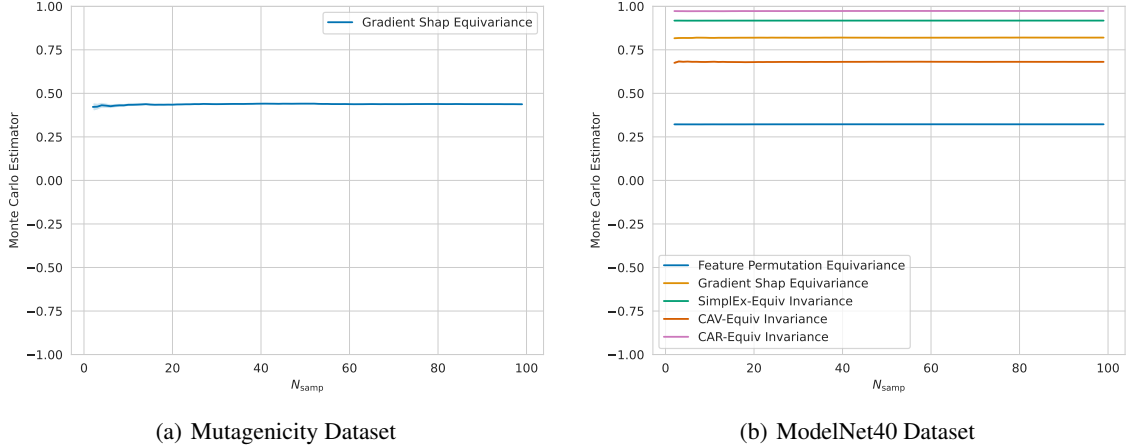


Figure 6: Convergence of the Monte Carlo estimators. Each curve represents the value of the estimator  $\widehat{\text{Inv}}_{\mathcal{G}}(e)$  or  $\widehat{\text{Equiv}}_{\mathcal{G}}(e)$  as a function of  $N_{\text{samp}}$ . In each case, we build a 95% confidence interval around this estimator.

**Symmetry Groups.** Each dataset in the experiment is associated to a specific group of symmetry and group representation. We detail those in Table 2. We note that all these groups and group representations are easily implemented as tensor operations on the dimensions of the tensor corresponding to the domain  $\Omega$ .

Table 2: Different groups and representations appearing in Section 3. Since Mutagenicity has heterogeneous graphs,  $V_x \subset \mathbb{N}^+$  denotes the set of vertices specific to the graph data  $x$ . We use the notation  $a(u, v)$  to denote the elements of the edges data matrix.

Dataset	Modality	Input Signal	Symmetry	Representation
Electrocardiograms	Time Series	$[x(t)]_{t \in \mathbb{Z}_T}$	$g \in Z/T\mathbb{Z}$	$\rho[g]x(t) = x(t - g)$
Mutagenicity	Graphs	$[x(u), a(u, v)]_{u, v \in V_x}$	$g \in S_{V_x}$	$\rho[g]x(u) = x(g^{-1}(u))$ $\rho[g]a(u, v) = a(g^{-1}(u), g^{-1}(v))$
ModelNet40	Tabular Set	$[x(n)]_{n \in \mathbb{Z}_{N_{\text{pts}}}}$	$g \in S_{N_{\text{pt}}}$	$\rho[g]x(n) = x(g^{-1}(n))$

**Data Split.** All the datasets are endowed with a natural train-test split. In the ECG dataset, the different types of abnormal heartbeats are imbalanced (e.g. fusion beats only amount for .7% of the training set). We use *SMOTE* [11] to augment the proportion of each type of abnormal heartbeat in the training set.

**Models.** We provide a detailed architecture for each model in Tables 3, 4, 5 and 6. All the models are implemented with *Pytorch* [54] and *PyG* [23]. All the models are trained using *Adam* [41]. The CNNs are trained to minimize the cross entropy loss for 200 epochs with early stopping and patience 10 with a learning rate of  $10^{-3}$  and a weight decay of  $10^{-5}$ . The GNN is trained to minimize the negative log likelihood for 200 epochs with early stopping and patience 20 with a learning rate of  $10^{-3}$  and a weight decay of  $10^{-5}$ . The Deep Set is trained to minimize the cross entropy loss for 1,000 epochs with early stopping and patience 20 with a learning rate of  $10^{-3}$ , a weight decay of  $10^{-7}$  and a MultiStepLR scheduler with  $\gamma = 0.1$ . The test set is used as a validation set in each case, as the model generalization is never used as an evaluation criterion. All the parameters hyperparameters that are not specified are chosen to the Pytorch and PyG default value. Note that for each architecture, we have highlighted the layer that we call *Inv* and *Equiv* in Section 3. The representation-based interpretability methods rely on the output of these layers.

**Model Invariance.** We note that Figure 4 includes *model invariance* on the  $x$ -axis. The metric we use to evaluate this invariance is simply adapted from Definition 2.1:  $\text{Inv}_{\mathcal{G}}(f, x) \equiv s_{\mathcal{Y}}[f(\rho[g]x), f(x)]$ , where  $s_{\mathcal{Y}} : \mathcal{Y}^2 \rightarrow \mathbb{R}$  is defined as  $s_{\mathcal{Y}}(y_1, y_2) = y_1^T y_2 / \|y_1\| \cdot \|y_2\|$  for all  $y_1, y_2 \in \mathcal{Y}$ . We note that this cos-similarity similarity metric is sensible in a classification setting since  $s_{\mathcal{Y}}(y_1, y_2) = 1$  implies  $y_1 = \alpha \cdot y_2$  for some  $\alpha \in \mathbb{R}^+$ . Since  $\|y_1\|_1 = \|y_2\|_1 = 1$ , this is equivalent to  $y_1 = y_2$ .

**Explanation Similarity.** In Definition 2.1, we also chose the cos-similarity metric  $s_{\mathcal{E}}[a, b]$  for two real-valued explanations  $a, b \in \mathbb{R}^{d_E}$ . This choice might seem arbitrary at first glance. By looking more closely, we notice that



Table 3: ECG All-CNN Architecture.

Layer Type	Parameters	Activation	Notes
Conv1d	in_channels=1, out_channels=16, kernel_size=3, stride=1, padding=1, padding_mode='circular'	ReLU	
Conv1d	in_channels=16, out_channels=64, kernel_size=3, stride=1, padding=1, padding_mode='circular'	ReLU	
Conv1d	in_channels=64, out_channels=128, kernel_size=3, stride=1, padding=1, padding_mode='circular'	ReLU	Equiv layer
Pooling	Global Average Pooling		
Linear	in_channels=128, out_channels=32	LeakyReLU	Inv layer
Linear	in_channels=32, out_channels=32	LeakyReLU	
Linear	in_channels=32, out_channels=2		

Table 4: ECG Augmented-CNN and Standard-CNN Architecture.

Layer Type	Parameters	Activation	Notes
Conv1d	in_channels=1, out_channels=16, kernel_size=3, stride=1, padding=1, padding_mode='circular'		
MaxPool1d	kernel_size=2		
Conv1d	in_channels=16, out_channels=64, kernel_size=3, stride=1, padding=1, padding_mode='circular'	ReLU	
MaxPool1d	kernel_size=2		
Conv1d	in_channels=64, out_channels=128, kernel_size=3, stride=1, padding=1, padding_mode='circular'	ReLU	Equiv layer
MaxPool1d	kernel_size=2		
Flatten	Collapse all the dimensions together except the batch dimension		
Linear	in_channels=2944, out_channels=32	LeakyReLU	Inv layer
Linear	in_channels=32, out_channels=32	LeakyReLU	
Linear	in_channels=32, out_channels=2		

$s_{\mathcal{E}}[a, b] = 1$  implies  $a = \alpha \cdot b$  for some  $\alpha \in \mathbb{R}^+$ . For all type of explanation that we consider in this paper,  $a$  and  $b$  will typically be vectors that aggregate various important scores (e.g. for each feature or training example). In practice, the scale of these importance scores does not matter. Indeed, if  $a = \alpha \cdot b$ , then the most important components will be the same for both  $a$  and  $b$ . Furthermore, the relative importance between any pair of component will be identical for both  $a$  and  $b$ . Therefore, we can consider that  $s_{\mathcal{E}}[a, b] = 1$  implies that both explanations are equivalent to each other  $a \sim b$ .

**Explanations.** For the feature importance methods, we use their *Captum* [44] implementation. All the other explanations methods are reimplemented based on their official repository and adapted to graph data. We note that some combinations of interpretability methods and models are impossible. We summarize and explain the incompatibilities in Table 7.

**Concepts.** We use a set of  $C = 4$  concepts for each dataset. For the ECG dataset, we use concepts defined by cardiologists to identify abnormal heartbeats: *Premature Ventricular*, *Supraventricular*, *Fusion Beats* and *Unknown*. We note that these concepts labels are directly available in the ECG dataset [35]. For the Mutagenicity dataset, we use the presence of known toxicophores [37] in the molecule of interest: *Nitroso* (presence of a N=O in the molecule), *Aliphatic Halide* (presence of a Cl,Br,I in the molecule), *Azo-type* (presence of a N=N in the molecule) and *Nitroso-type* (presence of a O<sup>+</sup>-N=O in the molecule). To detect the presence concepts, each molecule in the dataset is checked by using *NetworkX* [28]. For the ModelNet40 dataset, we use visual concepts whose presence can immediately be inferred from the class label: *Foot* (whether the represented object has a foot), *Container* (whether the represented object has the shape of a container), *Parallelepiped* (whether the represented object has a parallelepiped shape) and *Elongated* (whether the represented object is stretched in one direction).

**Concept Classifiers.** All the concept classifiers are implemented with *scikit-learn* [55]. We use training sets of size 200 for the ECG dataset and 500 for the Mutagenicity and ModelNet40 dataset. CAR classifiers are chosen to be SVCs with Gaussian RBF kernel and default hyperparameters. CAV classifiers are linear classifiers trained with stochastic gradient descent optimizer with a learning rate of  $10^{-2}$  and a tolerance of  $10^{-3}$  for 1,000 epochs. In the case of CAR classifiers, we found it useful to apply PCA with 10 principal components to reduce the dimension of the latent representation

Table 5: Mutagenicity GNN. The GraphConv layers correspond to the graph operator introduced in [51]

Layer Type	Parameters	Activation	Notes
GraphConv	in_channels=14, out_channels=32	ReLU	
GraphConv	in_channels=32, out_channels=32	ReLU	
GraphConv	in_channels=32, out_channels=32	ReLU	
GraphConv	in_channels=32, out_channels=32	ReLU	
GraphConv	in_channels=32, out_channels=32	ReLU	
Pooling	Global additive pooling on the graph		
Linear	in_channels=32, out_channels=32	ReLU	Inv layer
Dropout	p=0.5		
Linear	in_channels=32, out_channels=2	Log Softmax	

Table 6: ModelNet40 Deep Set adapted from [78]. The *Sub. Max* layers correspond to the operation  $x_{b,s,i} \mapsto x_{b,s,i} - \max_{s' \in \mathbb{Z}_{N_{\text{pt}}}} x_{b,s',i}$  for each batch index  $b \in \mathbb{N}$ , set index  $s \in \mathbb{Z}_{N_{\text{pt}}}$  and feature index  $i \in \mathbb{Z}_3$ .

Layer Type	Parameters	Activation	Notes
Sub. Max			
Linear	in_channels=3, out_channels=256	Tanh	
Sub. Max			
Linear	in_channels=256, out_channels=256	Tanh	Equiv layer
Sub. Max			
Linear	in_channels=256, out_channels=256	Tanh	
Max Pooling	Takes the maximum along the set dimension		
Dropout	p=0.5		
Linear	in_channels=256, out_channels=256	Tanh	Inv Layer
Dropout	p=0.5		
Linear	in_channels=256, out_channels=40	Tanh	

before applying the classification step. Indeed, this does not significantly reduce the accuracy of the resulting classifiers while significantly reducing the runtime.

## E Comparison with Sensitivity

In this appendix, we compare our robustness metric with the sensitivity metric introduced by [77]. This metric studies the robustness of an explanation with respect to a small perturbation in the input features. It is defined as follows:

$$\text{Sens}(e, x) = \max_{x' \in \mathcal{X}(\Omega, \mathcal{C})} \|e(x) - e(x')\|_2$$

$$\text{s.t. } \|x' - x\|_\infty \leq \epsilon,$$

where  $\|\cdot\|_\infty$  denotes the  $l_\infty$  norm,  $\|\cdot\|_2$  denotes the  $l_2$  norm and  $\epsilon \in \mathbb{R}^+$  is a small positive constant that is fixed to  $\epsilon = .02$  in the default Captum implementation of the metric. The rationale behind this metric is the following: a small perturbation of the input should have little impact on the model’s prediction and, hence, little impact on the resulting explanation as well. For this reason, one typically expects a low sensitivity  $\text{Sens}(e, x)$  for an explanation that is robust to small input shifts. We simply note that the previous reasoning is debatable due to the existence of adversarial perturbations that are small in norm but that have large effect on the model’s prediction [67].

Like our invariance and equivariance robustness metrics, Sens measures how the explanation is affected by a transformation of the input. Therefore, a natural question arises: is there a difference in practice between our robustness metrics and the sensitivity metric? To answer this question, we consider the setup of Section 3 with the ECG dataset and the Augmented-CNN. We study feature importance methods  $e$ , for which we evaluate  $\text{Sens}(e, x)$  and  $\text{Equiv}_{\mathcal{G}}(e, x)$  for  $N_{\text{test}} = 1,000$  test examples  $x \in \mathcal{D}_{\text{test}}$ . We report the results in Figure 7.

As we can observe on Figure 7, there exists a weak downward trend between the two metrics. By evaluating the Pearson correlation coefficient between the two metrics for each method, we found  $r = -.62$  for Integrated Gradients,

Table 7: Not all interpretability method can be used in all settings. We detail the exceptions here.

Method	Incompatible with	Reason
Feature Permutation	Mutagenicity	Heterogeneous graphs have different number of features.
Feature Occlusion	Mutagenicity, ModelNet40	Specific to CNNs.
SimplEx-Equiv	Mutagenicity	Heterogeneous graphs lead to equivariant representations with different dimensions.
Rep. Similar-Equiv	Mutagenicity	Heterogeneous graphs lead to equivariant representations with different dimensions.
CAV-Equiv	Mutagenicity	Heterogeneous graphs lead to equivariant representations with different dimensions.
CAR-Equiv	Mutagenicity	Heterogeneous graphs lead to equivariant representations with different dimensions.

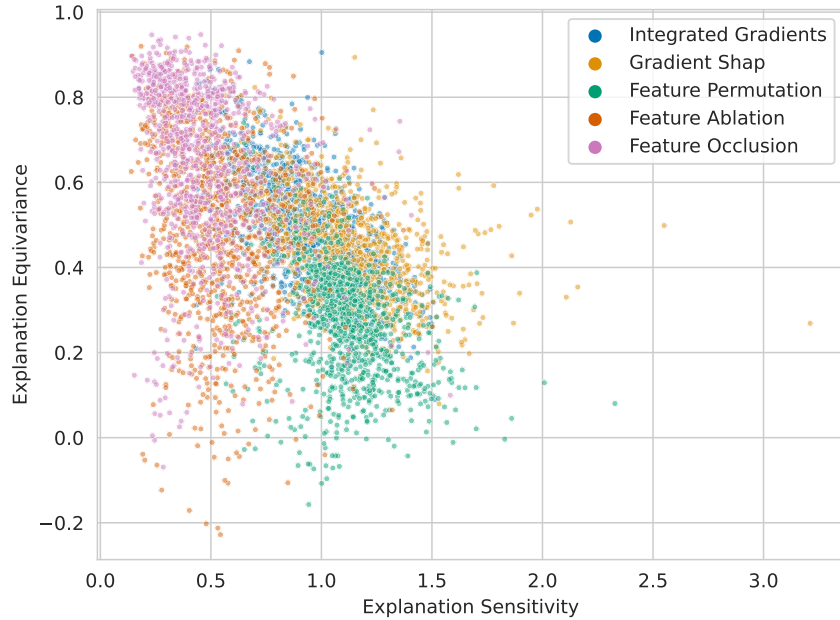


Figure 7: Comparison between the sensitivity metric  $\text{Sens}(e, x)$  and our equivariance metric  $\text{Equiv}_{\mathcal{G}}(e, x)$ . Each point represents a test example  $x \in \mathcal{D}_{\text{test}}$  extracted from the ECG dataset explained by a feature importance method  $e$ . The downward trend between the two metrics is weak.

$r = -.48$  for Gradient Shap,  $r = -.38$  for Feature Permutation,  $r = -.23$  for Feature Ablation and  $r = -.31$  for Feature Occlusion. This indicates that examples with higher sensitivity tend to be associated with lower equivariance. That being said, the correlation between the two metrics is too weak to suggest any redundancy between them. We deduce that our robustness metrics should be use to complement rather than replace the sensitivity metric. In practice, we believe that many forms of explanation robustness deserve to be investigated.

## F Other Invariant Architectures

In Section 3, we have illustrated the flexibility of our robustness formalism by applying it to various architecture. However, geometric deep learning extends well-beyond the examples covered in this paper and an exhaustive treatment of the field is beyond our scope. To suggest future extensions of our work beyond the architectures examined in this paper, we provide in Table 8 other architectures that are invariant or equivariant with respect to other symmetry groups. Our formalism straightforwardly applies to most of these examples. For some others (like Spherical CNNs), an extension to infinite groups would be required. We leave this extension for future work.

Table 8: Other invariant architectures. Table partially adapted from [10].

<b>Architecture</b>	<b>Symmetry Group <math>\mathcal{G}</math></b>	<b>Reference(s)</b>
G-CNN	Any finite group	[15]
Transformer	Permutation $S(n)$	[33]
LSTM	Time Warping	[68]
Spherical CNN	Rotation $SO(3)$	[16]
Mesh CNN	Gauge Symmetry $SO(2)$	[30]
$E(n)$ -GNN	Euclidean Group $E(n)$	[61, 7]